THE GEOLOGICAL SOCIETY OF AMERICA®

Late Holocene rupture behavior and earthquake chronology on the Hope fault, New Zealand

Narges Khajavi[1,†], Robert M. Langridge[2], Mark C. Quigley[1,§], Chris Smart[3], Amir Rezanejad[4], and Fidel Martín-González[5]

[1]*Department of Geological Sciences, University of Canterbury, Christchurch, 8140, New Zealand*
[2]*GNS Science, Lower Hutt, Wellington, 5040, New Zealand*
[3]*Department of Geography, University of Western Ontario, London, Ontario N6A 5C2, Canada*
[4]*Department of Civil and Natural Resources Engineering, University of Canterbury, Christchurch, 8140, New Zealand*
[5]*Área de Geología, Escuela Superior de Ciencias Experimentales y Tecnología (ESCET), Universidad Rey Juan Carlos, 28933 Móstoles, Spain*

ABSTRACT

The Hope fault is the most active and southernmost splay of the Marlborough fault system in the northern South Island of New Zealand. The fault consists of five geometrically defined segments. We used trenching to acquire paleoseismic data and radiocarbon dating of faulted late Holocene sediments on the Hurunui segment of the Hope fault to derive an earthquake chronology that extends from the historic 1888 M_w 7.1 Amuri earthquake to ca. 300 C.E., thereby providing the longest chronologic record of earthquakes on the Hope fault to date. Earthquake event horizons were identified by upward fault terminations, colluvial wedges, unconformities, and/or progressive folding of shutter basin deposits. Six earthquakes identified at C.E. 1888, 1740–1840, 1479–1623, 819–1092, 439–551, and 373–419 indicate a mean recurrence interval of ~298 ± 88 yr, with successive median interevent times ranging from 98 to 595 yr. The large variance in interevent times with respect to mean recurrence interval is explained by (1) possible coalescence of rupture overlap from the adjacent Hope River segment onto the Hurunui segment at our study site (including the 1888 Mw 7.1 Amuri earthquake, sourced primarily from the Hope River segment), which results in apparently shorter interevent times at the study site compared to mean recurrence intervals from adjacent fault segments, (2) possible earthquake temporal clustering on the Hurunui segment, which could result in interevent times that are significantly shorter or longer than interevent times and mean recurrence intervals predicted by a periodic earthquake rupture model, and/or (3) "missing" events, which could result in interevent times and mean recurrence intervals at the study site that are longer than the actual mean recurrence interval. While we cannot exclude option 3 as a possibility, we prefer options 1 and 2 to explain earthquake chronologies and rupture behavior on the Hurunui segment of the Hope fault, given the detailed nature of our geologic and chronologic investigations. By demonstrating that the 1888 Amuri earthquake propagated through a proposed segment boundary, we provide the first evidence for coseismic multisegment ruptures on the Hope fault. In contrast, the penultimate earthquake ruptured the Hurunui segment at 1740–1840 C.E. with no known rupture of the Hope River segment. Paleoearthquake records near geometrically complex segment structural boundaries on major strike-slip faults may show temporal recurrence distributions resulting from earthquake ruptures that variably arrest or propagate through proposed segment boundaries. We note that earthquake recurrence along major strike-slip plate-boundary faults may vary between more periodic and more episodic end members, even on adjacent, geometrically defined segments.

INTRODUCTION

Earthquake moment magnitude (M_w) varies proportionately with the source rupture area (length × width) and average coseismic displacement (e.g., Kanamori, 1977; Wells and Coppersmith, 1994; Leonard, 2010). Trenching of faults can be used to document the rupture lengths and coseismic displacements of historic and prehistoric earthquake faults to determine past earthquake M_w for integration into seismic hazard models (e.g., McCalpin, 2009). However, the interpretation of paleoseismic trench data and event chronology can be complicated due to: (1) the complex nature of fault ruptures propagating through heterogeneous sediment packages (Quigley et al., 2012); (2) variable topography (Khajavi et al., 2014) and surface processes that can lead to incomplete, spatially variable, or ambiguous evidence for earthquake events, even for structurally mature faults of different lengths (Scharer et al., 2007; Hartleb et al., 2003, 2006); and (3) rupture segmentation on large strike-slip fault systems, which are typically composed of multiple segments with intervening stepovers or bends that can impede rupture propagation (Wesnousky, 1988, 2006; Oglesby, 2005; Elliott et al., 2009). Also, slip distributions from earthquake ruptures on adjacent fault segments may overlap, resulting in repeat rupture at the overlapping zone over relatively short time frames (i.e., months to decades), as compared to expected return times of major earthquakes on individual faults segments. Examples of this are: the 1999 Izmit and Düzce earthquakes (Hartleb et al., 2002; Langridge et al., 2002), 1939 and 1951 Erzincan earthquakes, 1939 and 1942 earthquakes on the North Anatolian fault (Barka, 1996, 2002), 2013 Scotia Sea earthquakes (Vallée and Satriano, 2014), and 1812 and 1857 San Andreas earthquakes (Weldon et al., 2005). Therefore, fault re-rupture due to overlapping slip from adjacent ruptures may introduce disorder into the apparent recurrence intervals of earthquakes (Ben-Zion and Rice, 1995), and thus prevent

†narges.khajavi@canterbury.ac.nz
§Present address: School of Earth Sciences, University of Melbourne, Melbourne, Victoria 3010, Australia.

GSA Bulletin; doi: 10.1130/B31199.1; 15 figures; 7 tables; Data Repository item 2016174.

discrimination of periodic versus clustered earthquake recurrence intervals (Grant and Sieh, 1994; Rockwell et al., 2000). Variations in the extent to which ruptures overlap along segmented active faults may result in apparent contradictions in paleoseismic earthquake chronologies along the length of these faults (Seitz et al., 1997, 2013; Fumal et al., 2002; Hartleb et al., 2003; Biasi and Weldon, 2009). In order to better constrain our understanding of rupture behavior, robust earthquake records proximal to geometrically defined fault segment boundaries are needed to compare with earthquake records from central parts of fault segments.

The Hope fault is one of the longest (~230 km) and fastest-slipping (~8–27 mm/yr) active faults in New Zealand (Fig. 1B; Cowan and McGlone, 1991; Langridge et al., 2003, Langridge and Berryman, 2005). Field, aerial photographic, and light detection and ranging (LiDAR) mapping (McKay, 1890; Freund, 1971; Cowan, 1989; Langridge et al., 2003, 2013; Langridge and Berryman, 2005; Beauprêtre et al., 2012; Khajavi et al., 2014) indicates that the Hope fault is highly segmented. The fault consists of five geometrically defined segments (from west to east: Taramakau, Hurunui, Hope River, Conway, and Seaward) of ~20–70 km length that are separated by fault stepovers of up to ~7 km (Figs. 1–2) and >15° changes in strike. Evidence for segmented rupture behavior along the Hope fault includes: (1) the 1888 Mw 7.1 Amuri earthquake, which ruptured the Hope fault for an estimated length of 13–150 km (6%–65% of total Hope fault length; McKay, 1890, 1902; Berryman, 1984; Knuepfer, 1984; Cowan, 1991); (2) along-fault variations in slip rate (e.g., ~8–15 mm/yr on the Hurunui segment, ~10–17 mm/yr on the Hope River segment, and ~19–27 mm/yr on the Conway segment); and (3) along-fault variations in the timing and estimated recurrence interval of paleoearthquakes (i.e., ~81–500 yr; Cowan and McGlone, 1991; Langridge et al., 2003; Langridge and Berryman, 2005). Thus, available data make the best possible estimates of the seismic hazard for the Hope fault very uncertain. The geometry of the Hope fault system suggests a segmentation model maybe viable; however, it is unclear whether the segmentation model is useful for estimating seismic hazards on the Hope fault.

In this paper, we report new data that could lead to an improved geologic basis for hazard estimation. In detail, digital elevation models (DEMs) derived from LiDAR and photogrammetry are used to better constrain the surface rupture morphology of the eastern end of the Hurunui segment of the Hope fault adjacent to the proposed segment boundary with the Hope River segment (Cowan, 1991; Langridge et al., 2013). Historical accounts of the 1888 Amuri earthquake (McKay, 1890) are reinterpreted in conjunction with our observations to determine a more accurate surface rupture length and location in relation to the Hope River and Hurunui segments. Two closely spaced (~4 m apart) trenches were excavated at the study site. Radiocarbon dating and OxCal modeling were used to investigate the timing of the past events at the study site, and dendrochronology and optically stimulated luminescence (OSL) dating were used to determine the age of the earthquake-displaced sedimentary deposits in order to further refine the timing of paleoearthquakes. These results were combined with new off-fault data, and previously published paleoseismic trenching data to compare earthquake chronologies on the Hope River and Hurunui segments. The extent to which the proposed geometric boundary between these segments terminates or impedes rupture propagation on the Hope fault is investigated, and implications for paleoseismic studies and rupture behavior are discussed.

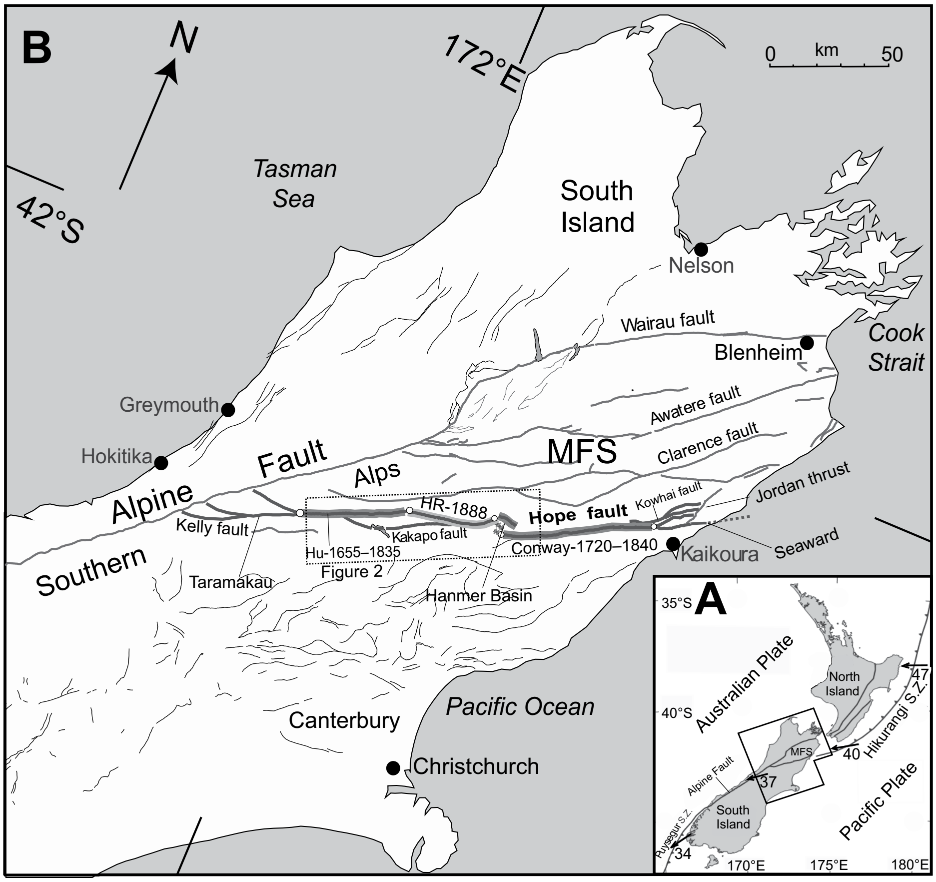

Figure 1. Geological setting of New Zealand and active faults in the northern South Island. (A) New Zealand plate boundary including subduction zones and major faults. Nuvel-1 plate rates (mm/yr) and orientations are after DeMets et al. (1994). S.Z.—shear zone. (B) Location of active faults within the northern South Island are shown; Marlborough Fault System (MFS) and the Alpine fault are highlighted; and the Hope fault is heavily highlighted; modified from Langridge and Berryman (2005). The timings of the most recent events along the Hurunui, Hope River, and Conway segments are presented in yr C.E., and their related segments are colored in gray bold (with historic event) and black bold (with known event). Box shows area of Figure 2.

TECTONIC SETTING AND BACKGROUND

Hope Fault and Marlborough Fault System

New Zealand occurs at the boundary between the Australian and Pacific tectonic plates in the SW Pacific. Nearly pure strike-slip motion occurs along the Marlborough fault system in the northern South Island at rates of ~39–48 mm/yr (Fig. 1; DeMets et al., 1994, 2010; Beavan et al., 2002; Yeats and Berryman, 1987;

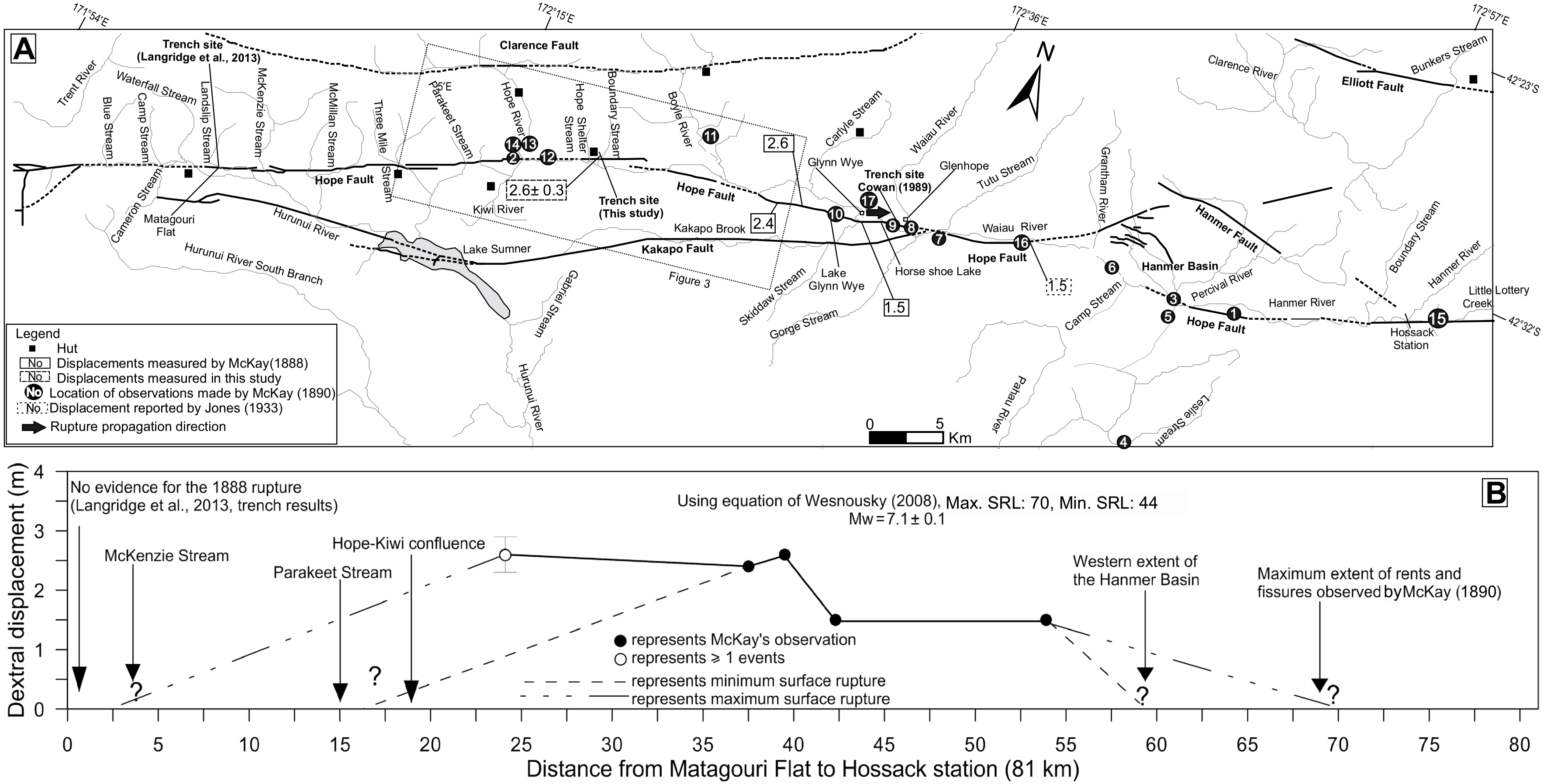

Figure 2. Observations of McKay (1890) mapped. (A) Geographical map showing the location of observations (1–16), certain (solid black lines) and uncertain (dashed lines) faults, trench sites, and measured along-fault slips. McKay's quotes related to his observations are presented in Appendix 1. (B) Slip distribution associated with the 1888 event. Eastern and western extents of the surface rupture were estimated using McKay's observations and the results of Langridge et al. (2013), and this study. SRL—Surface rupture length.

Berryman and Beanland, 1991; Van Dissen and Yeats, 1991; Pettinga et al., 2001; Wallace et al., 2007, 2012). The Marlborough fault system consists of four major dextral strike-slip faults: the Wairau, Awatere, Clarence, and Hope faults, which transfer the motion between the Alpine fault in the west and the Hikurangi subduction zone in the east (Fig. 1B).

The ENE-striking Hope fault is the youngest (initiated ca. 1–2 Ma) and southernmost fault in the Marlborough fault system (Freund, 1971; Van Dissen, 1989; Cowan, 1990; Wood et al., 1994; Langridge and Berryman, 2005), and it has the second highest slip rate among onshore faults in New Zealand. The Hope fault is segmented (Langridge et al., 2013) and includes branching faults (Kelly, Kakapo, and Kowhai faults), pull-apart basins, stepovers, and structural bends (Fig. 1B; Yang, 1991; Van Dissen and Yeats, 1991; Pettinga et al., 2001; Berryman et al., 2003). Movement along strike-slip segments of the fault has developed transpressional duplexes (Eusden et al., 2000, 2005), and pull-apart basins such as Hanmer Basin (Figs. 1 and 2), one of the best known examples of a depression formed at a releasing stepover (Wood et al., 1994). Typically, the Hope fault constitutes an ~1.3-km-wide deformation zone including depressions, folds, and wedges that have previously been documented or structurally investigated along the length of the fault (Freund, 1971; Cowan, 1989; Eusden et al., 2000, 2005; Khajavi et al., 2014). Measured slip rates along the fault indicate that it accommodates nearly half of the plate-tectonic motion across the Marlborough region (Cowan, 1990; Cowan and McGlone, 1991; Van Dissen and Yeats, 1991; Knuepfer, 1992; Langridge et al., 2003; Langridge and Berryman, 2005).

1888 Amuri Earthquake: Background and Reassessment of McKay's Observations

On 1 September 1888, a large earthquake (termed the North Canterbury or Amuri earthquake) occurred on the Hope fault (McKay, 1890, 1902). That earthquake ruptured the Hope River segment of the fault and produced displacements ranging from 1.5 to 2.6 m (Fig. 2; McKay, 1890; Cowan, 1991). Estimations of the true extent of the 1888 Amuri surface rupture range from 13 km (from the Hope-Boyle confluence to the Hope-Waiau confluence) to 150 km (from the junction of the Alpine and Hope faults to the east of Hanmer Basin; McKay, 1890, 1902; Berryman, 1984; Knuepfer, 1984). Cowan (1991) argued that the rupture length was probably 30 ± 5 km from the Hope-Boyle confluence to the Hanmer Basin (Figs. 1 and 2), based on the observed and reported damage and reports of aftershock concentration patterns. He also argued that the rupture was initiated beneath the Hope-Boyle confluence (Fig. 2), which was considered to be a 4-km-wide tectonic basin formed at a releasing bend along the Hope fault (Clayton, 1966). Estimates of the moment magnitude of the Amuri earthquake are M_w 7–7.3 (Cowan, 1991), and M_w 7.1 (Stirling et al., 2012).

The postearthquake observations of McKay (1890; see Appendix 1 herein), and subsequent interpretations of earthquake rupture length (Berryman, 1984; Knuepfer, 1984; Cowan, 1991) provide important information relevant to our study. Our trench site (Figs. 2 and 3) falls along the known or suspected zone of faulting associated with the 1 September 1888 Amuri earthquake. McKay's report includes terms such as "line of greatest disturbance," "line of greater dislocation," "earthquake-fracture," "old and new earth-fractures," "ground-rents," "earth-rents," "fissures," "slips," "rents and openings," "old line of dislocation," "recently-formed earth-rents," "recently-formed fractures," "old earthquake-rents," "traces of earthquake-action" to describe both the prehistoric (pre-1888) and the 1888 Amuri earthquake-induced surface features (Appendix 1). McKay clearly distinguishes the 1888 Amuri surface fractures resulting from fault rupture (e.g., "line of dislocation or greatest disturbance," "earthquake fracture or rents"), ground failure (e.g., "rents," "opening," "slips," "fissures"), and those for which no specific origin is inferred (e.g., "ground-rent," "earth-rent"). In this study, we interpret the terms "line of greater dislocation," "line of greatest disturbance," and "earthquake-fracture" to refer to a surface rupture (Appendix 1: 1, 2, and 14), and the term "old line of dislocation" to refer to a former surface rupture (Appendix 1: 1, 10, and 15). The term "slip" is commonly used in New Zealand to refer to a landslide (Appendix 1: 1, 4, 10, 13, and 14), so we do not interpret those as fault slips. Figure 2 shows documented observations and measured single-event displacements between the Hope-Kiwi area and Hanmer Plain, which encompasses parts of both the Hurunui and Hope River segments. Quotes from the words of McKay (1890), which are related to locations 1–16 and displacements identified in Figure 2, appear in Appendix 1.

Based on McKay's observations and comments, it can be inferred that: (1) the clearest evidence of the western limit of the 1888 Amuri surface rupture was near the Hope-Kiwi confluence (Fig. 2; Appendix 1: 2 and 15); and (2) its eastern limit was identified by rents and fissures at the eastern end of the Hanmer Plain, but not as far as the area between the Hanmer River and Lottery Creek (Fig. 2; Appendix 1: 15). In his opinion, the 1888 Amuri surface rupture com-

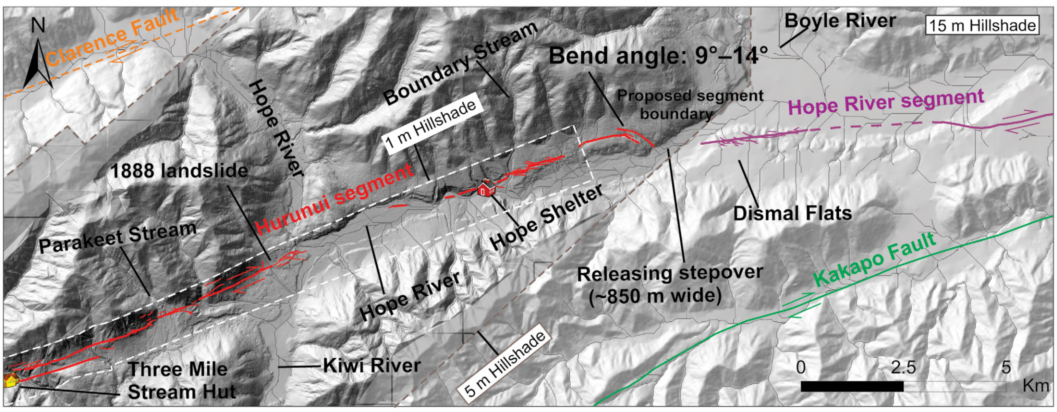

Figure 3. Structural map of the western Hope fault, including the overlapping area of the two segments. Locations of the fault bend and releasing stepover are shown in between the two segments. Defined western extension of the 1888 rupture (Cowan, 1989) is shown (purple line). Location of the 1888 landslide (McKay, 1890) is shown on the map near the Hope-Kiwi confluence.

menced at some point to the west of Glynn Wye (maybe even farther west than the Hope-Kiwi confluence) and propagated to the east with increasingly strong ground motions to Glynn Wye and Glenhope, with decreased ground damage from Glenhope toward the eastern end of the Hanmer Plain (Appendix 1: 15). McKay mentioned the earthquake fracture, snapped, broken, and thrown-down trees, and a possible continuation of the fault for a mile or more into the forest west of the Hope-Kiwi confluence (location 2 on Fig. 2; Appendix 1: 13).

These observations conflict with the interpretations of Cowan (1991), who placed the western limit of the surface rupture at the Hope-Boyle confluence (Fig. 2). Based on our reinterpretation of McKay's account (1890), the most reasonable interpretation is that the 1888 Amuri earthquake is likely to have ruptured through our trench site in the Hope Valley. This hypothesis is examined further in this study. Figure 2 highlights the surface slip distribution associated with that event, shows our reinterpretation of the fault rupture length, and adds one slip measurement near our trench site to the slip gradient.

Paleoseismicity of the Hope Fault

The spatial and temporal patterns of large earthquakes on the Hope fault are uncertain due to the scarcity of historical records (starting from ca. 1840 C.E.; Langridge et al., 2013), and the difficulty in undertaking paleoseismic investigations in the mountainous terrain through which the fault passes. Langridge et al. (2003) measured the cumulative and single-event displacements on the surface near their trench sites on the eastern Conway segment and used the radiocarbon dates obtained from trenches to conclude that the Conway segment has a recurrence interval of 180–310 yr and is capable of generating $\geq M_w$ 7 earthquakes. Beauprêtre et al. (2012) measured the surface and subsurface displacements using three-dimensional ground-penetrating radar (GPR) and LiDAR to analyze part of the Conway segment. Their results suggested that the Conway segment has a mean recurrence interval of ~200 yr and can generate earthquakes with magnitudes of at least M_w 7–7.4. Langridge and Berryman (2005) measured surface displacements using traditional techniques (tape measure, compass, handheld global positioning system [GPS]), and dated surfaces using radiocarbon samples to estimate the fault parameters. Their results revealed that the Hurunui segment has an average recurrence interval of 310–490 yr and is capable of generating M_w 7.2–7.4 earthquakes.

Cowan and McGlone (1991) excavated a trench across the Hope River segment and interpreted that five temporally characteristic (i.e., periodic) events (including the Amuri earthquake) with an average recurrence interval of ~140 yr occurred on the Hope River segment during the last 700 yr (Table 1). Langridge et al. (2013) subsequently reinterpreted Cowan's trench and argued that only two events had ruptured the Hope River segment during the last ~400–900 yr (Table 1). Trenching investigations on the eastern Conway and western Hurunui segments by Langridge et al. (2003, 2013) did not show any evidence of rupture by the 1888 Amuri earthquake but did show evidence for two events in the last ~600 yr on the Hurunui segment, and three events in the last ~800 yr on the Conway segment (Table 1).

Geomorphology of the Hope Fault

The bedrock lithology consists primarily of sandstones, mudstones, and mélange collectively grouped as the Torlesse composite terrane of Triassic age (Nathan et al., 2002). During the Last Glacial Maximum (LGM, Otira glaciation, ~18,000 yr ago; Nathan et al., 2002), the Hope Valley was filled by ice. As the glaciers retreated, the Hope Valley was partly infilled with sediments deposited by glacial meltwater and/or adjoining alluvial fans. During the Holocene, rivers have incised into these aggradational surfaces, creating suites of fluvial terraces (Barrell and Townsend, 2012). Glaciofluvial, alluvial, and landslide/debris deposits of late Pleistocene to Holocene age comprise the majority of post-LGM sediment in the valley (Langridge et al., 2013).

The approximate location of the main trace of the Hope fault appeared on early regional geological maps (Lensen, 1962; Bowen, 1964; Gregg, 1964; Warren, 1967), and a more detailed fault trace appeared on later regional geological maps (Nathan et al., 2002; Rattenbury et al., 2006). Cowan (1989) used aerial images and field observations, and Khajavi et al. (2014) used airborne LiDAR, photogrammetry, and field observations to produce detailed maps of the fault zone along the Hope River and Hurunui segments of the Hope fault, respectively. Figure 3 presents a simplified version of the main fault traces and structural complexities between the Hurunui and Hope River segments. Based on the numerous en echelon structures identifiable on the LiDAR DEM located near the eastern end of the Hurunui segment on the north side of the Hope River, Khajavi et al. (2014) argued that this area may represent a damage zone linking the two fault segments (Fig. 3).

METHODOLOGY

Background, Fault Mapping, and Site Selection

No paleoseismic studies have been conducted in the area proposed to be the segment boundary between the Hope River and Hurunui segments (Fig. 3). For this reason, this study focused on the eastern end of the Hurunui segment, including the area of the proposed segment boundary (Fig. 1; McKay, 1890; Cowan, 1991; Langridge and Berryman, 2005; Langridge et al., 2013). Along the Hurunui segment, native beech (*Nothofagus*) forest covers and obscures much of the fault trace and underlying morphology (Langridge and Berryman, 2005; Langridge et al., 2013, 2014). Documentation of the surface rupture attributes of the fault was thus required for identifying the best sites for trenching. Airborne LiDAR was used (see also Langridge et al., 2014; Khajavi et al., 2014) to extract accurate surface topography from beneath forest cover. The LiDAR survey did not cover the entire area between the Hope River and Hurunui segments in its eastern extent, and thus high-resolu-

TABLE 1. KNOWN PALEOSEISMIC HISTORIES ALONG SEGMENTS OF THE HOPE FAULT

Segments	Events and timing (C.E.)	Reference
Hurunui	Two events in the last ~600 yr 1655–1835 and 1425–1625	Langridge et al. (2013)
Hope River	Rive events in the last ~700 yr 1888,1745, 1602,1459, 1316	Cowan (1989), Cowan and McGlone (1991)
Hope River: reinterpreting Cowan's trench data and using OxCal to recalculate the events timing	From the five events (i.e., 1888, 1654–1844, 1565–1829, 1443–1718, and 1118–1609), only two were surface faulting events (i.e., 1888 and 1118–1609) in the last ~900 yr, and the rest were shaking events	Langridge et al. (2013)
Conway	Three events in the last ~800 yr 1720–1840, 1295–1405, before 1220	Langridge et al. (2003)

tion photogrammetry was used to map potential fault traces in the area where the two segments overlap. Georectified aerial photographs (taken in November 2008) covering the same area as LiDAR plus an extra ~4.5 km of coverage to the east, and SOCET (SOftCopy Exploitation Toolkit) GXP(Geospatial eXploitation Product) 3.2 photogrammetry software were used to create a 5 m DEM and associated hillshade model (Fig. 3; Khajavi et al., 2014).

We mapped fault traces near the segment boundary using three overlapping hillshade models (derived from the 2 m LiDAR, the 5 m SOCET GXP, and an existing national coverage 15 m DEMs; Fig. 3). In the overlapping area of the two segments, an ~850-m-wide right stepover in the fault associated with an ~9°–14° degree fault bend was discovered (Fig. 3). Khajavi et al. (2012) surmised that this bend and stepover could play an important role in influencing the dynamics and extent of rupture termination or propagation (e.g., in the 1888 Amuri earthquake). Based on the above, we selected a site for paleoseismic study at the eastern end of the LiDAR swath and named it "Hope Shelter" (due to its proximity to the Hope Shelter hut in the middle Hope Valley; Figs. 2 and 3). The Hope Shelter site proved an optimal location for trenching the fault because of the single sharp linear fault trace that blocked a natural drainage, creating a swamp with a potential source of datable material. The site was also selected because of its sparse vegetation.

Two narrow (<1-m-wide) trenches were excavated at the Hope Shelter site (Figs. 4B and 5A–5F). Trench 1 (T-1; 9 m long by 1 m deep; Figs. 6, 7, and 8) was excavated in February 2012 by backhoe across the shutter ridge within a small wind gap (formed by an abandoned channel; Fig. 5A). At this location, the scarp height is ~0.5 m, and the width of the swampy basin is ~10 m. Trench T-1 was located ~50 m from the western edge of the debris deposit (Fig. 4). T-1 had a branch trench (we named "pit 1"; Fig. 5A), which was excavated within the wind gap in the scarp to understand the geometry and age of any channelized deposits within it (see Fig. DR3).[1] Trench 2 (T-2, ~2.5 m long and 1.3 m deep; Figs. 7 and 9) was excavated by hand in February 2013 in an attempt to understand some of the stratigraphic and age anomalies observed

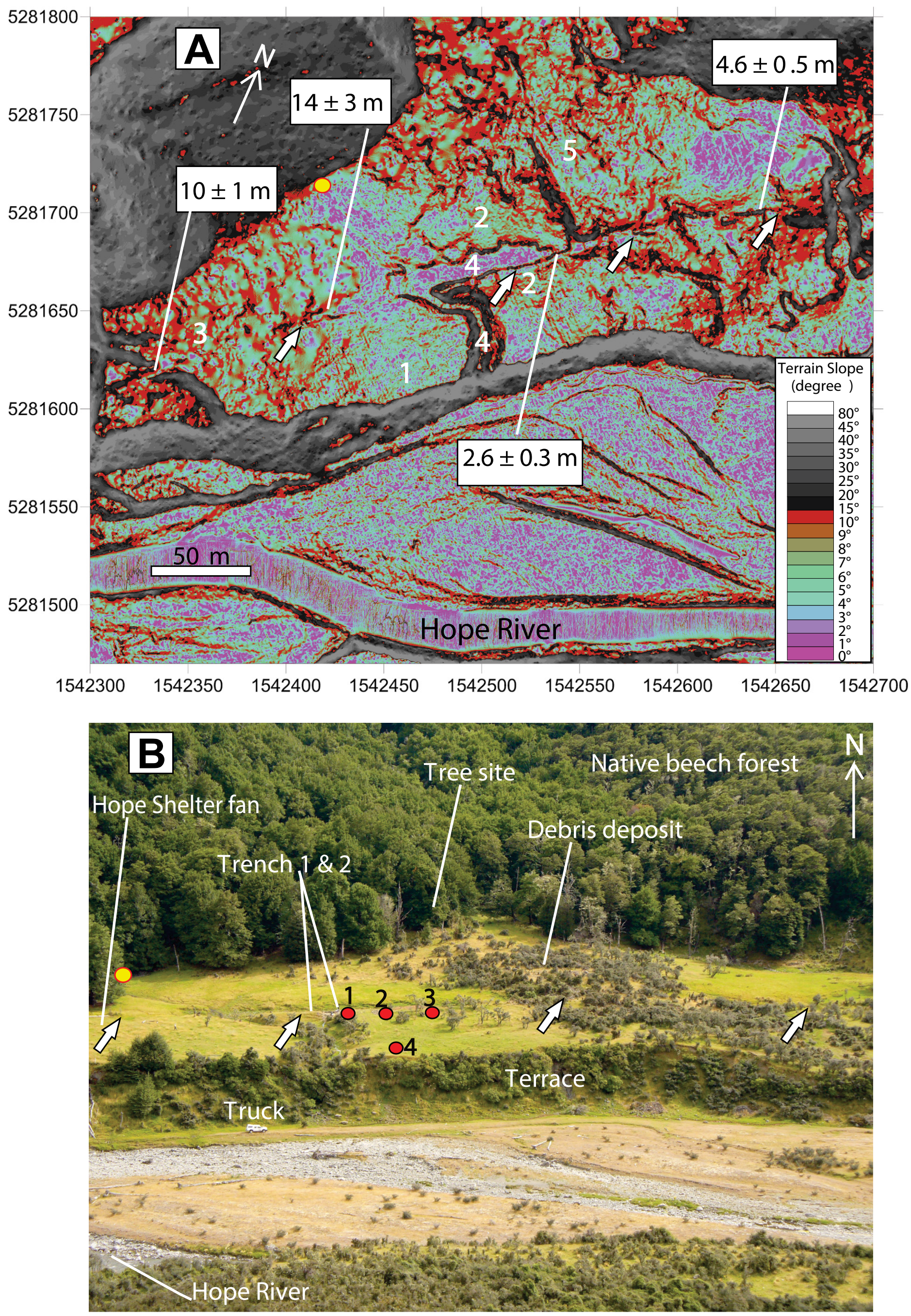

Figure 4. Details of the Hope Shelter site. (A) 0.1 m slope map, which is made up of the 1 m light detection and ranging (LiDAR) digital elevation model (DEM). Morphologies of the five features are identifiable by different surface slopes. Numbers on the map are: 1—terrace, 2—trench site fan, 3—Hope Shelter fan, 4—channel and shutter basin, and 5—debris deposit. Locations of the measured displacements and the hot spring (yellow solid circle) are shown. (B) Photograph showing the five geomorphic features, trench 1 and trench 2, pit locations (1–4; red solid circles), hot spring, and our tree site (where our dendrochronologic work was carried out). Arrows point to the fault trace. Projected coordinate system for X and Y: New Zealand Transverse Mercator 2000 (NZTM 2000).

[1]GSA Data Repository item 2016174, (1) An example of peat sample, (2) and (3) Details of the Matagouri bush and pit logs at the Hope Shelter site, (4) Details of the Schmidt hammering technique, (5) Location of the fault structures near the segment boundary, (6) Parakeet Stream data, and (7) Details of calculating mean recurrence interval (MRI), is available at http://www.geosociety.org/pubs/ft2016.htm or by request to editing@geosociety.org.

A: Trench 1
B: Trench 2
C: Trench 2; overall log
D: Trench 2; deformed units
E: Trench 1; shutter scarp vs. shutter basin deposits
F: Trench 1; deformation of the shutter basin deposits

PSZ: Principal Slip Zone

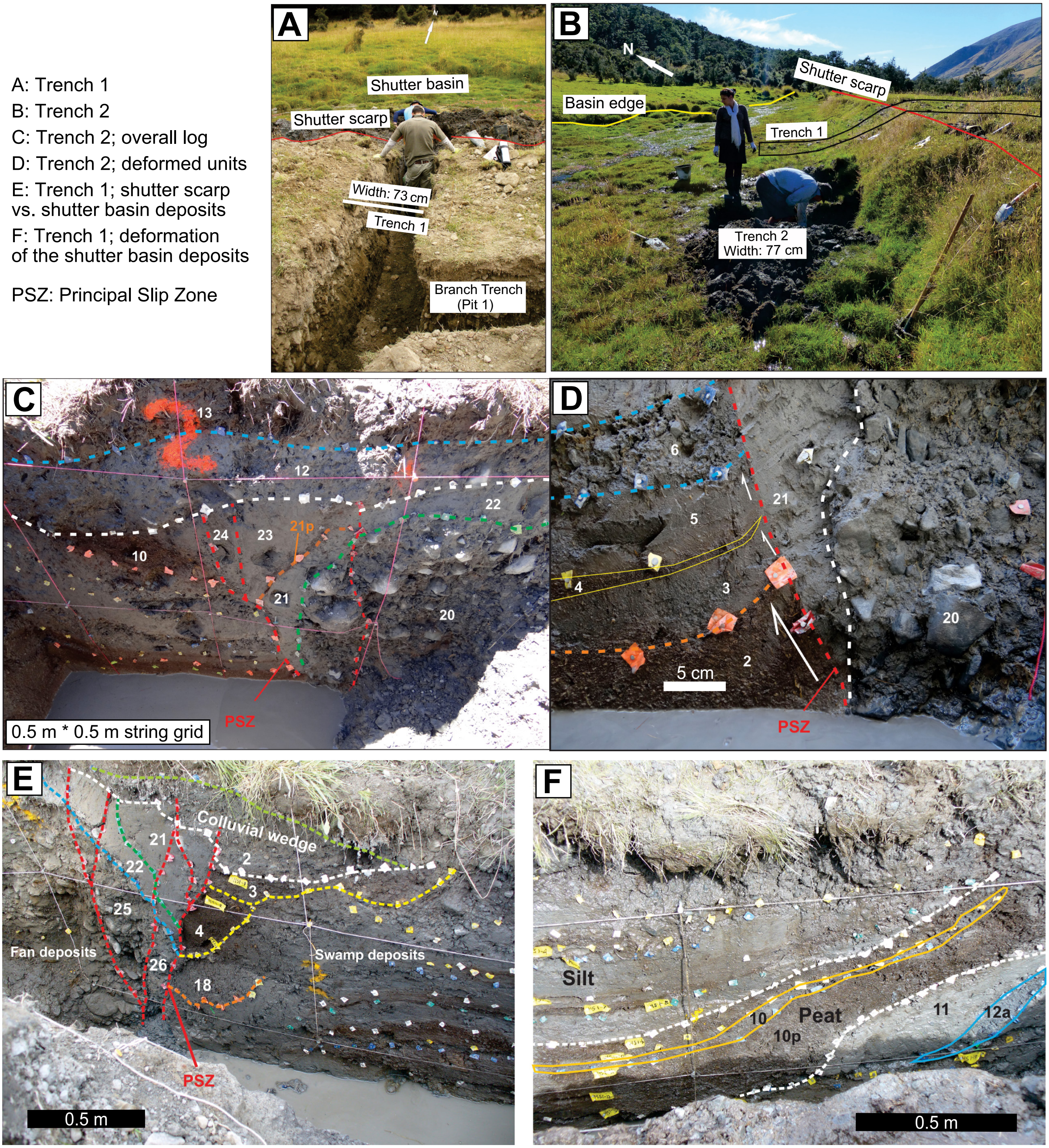

Figure 5. (A–B) Trench T-1 and trench T-2 pictures and (C–F) photo-logs. Numbers represent units (see Appendix 2 for details).

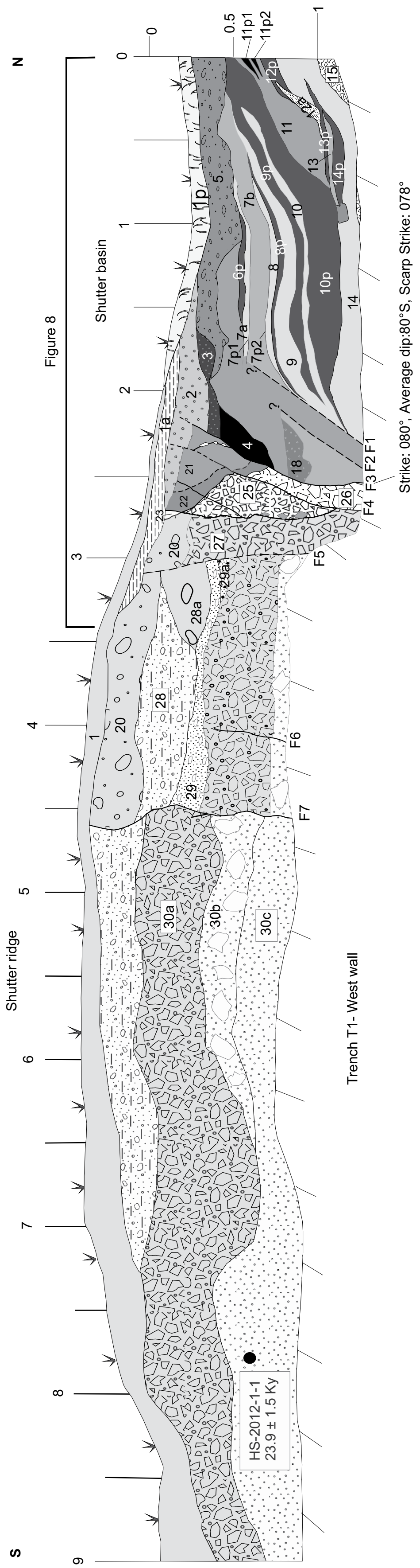

Figure 6. The full log of trench T-1. Trench wall was logged at a scale of 1:10. From meters 2.5–9, fan gravels are prevalent and are faulted near the fault scarp. From meter 0 to meter 2.5, swamp deposits are juxtaposed against the fan deposits and are either faulted or deformed. See Appendix 2 for unit descriptions.

from T-1 (Figs. 5C–5D). T-2 was excavated into the scarp and shutter basin deposits adjacent to T-1. At this location, the scarp was steep, with a height of ~1.1 m. The width of the swampy basin there is ~7 m. The log of the east wall of T-2 (Fig. 9) was supplemented by several auger holes to extend the depth and continuity of units. Both trenches were limited in their extents into the shutter basin by the presence of flowing water at the ground surface (Figs. 6 and 8).

Dating Techniques

Various dating techniques were applied to see whether they could help to constrain the prehistoric and 1888 rupture earthquakes. These techniques are: (1) radiocarbon dating on organic samples from two on-fault trenches excavated across the fault scarp at the Hope Shelter site and four off-fault auger holes at swamps south of the fault near Parakeet Stream (see Figs. 2–4; Figs. DR9–DR10 [see footnote 1]); (2) OSL dating on samples of sand and silt from the Hope Shelter site, extracted from one of the trenches on the shutter ridge fan and a pit excavated into the Holocene terrace (see Fig. 4; Fig. DR5 [see footnote 1]); (3) Schmidt hammer "rebound values" (e.g., Stahl et al., 2013), to calibrate the age of the debris deposit relative to a pre-1888 debris deposit at the Hope-Kiwi confluence (see Part 4 in the Data Repository material [see footnote 1]); and (4) dendrochronology on trees and bushes at the Hope Shelter site. Native beech trees are absent in the central part of the site; however, Matagouri (*Discaria toumatou*) scrub is abundant on the debris deposit (Fig. 4B). Despite having wide trunks, Matagouri bushes are substantially younger than the 1888 Amuri earthquake event. According to a tree-ring count conducted as part of this study, the age of the sampled bush was 82 yr (1930) (see Fig. DR2 [see footnote 1]). We found no documentation to confirm that the central part of the site might have been deforested by pastoralists. However, uphill and surrounding the site, big red beech (*Nothofagus fusca*) trees have colonized the upper end of the debris deposit at the mouth of the gully (Fig. 4B), and dendrochronology was used to date the trees growing on the upper side of the debris deposit (see Fig. 4B for location).

OxCal Modeling of Radiocarbon Ages

In order to develop a refined chronology of paleoseismic events at the Hope Shelter site, a Bayesian statistical approach that draws on the strengths of stratigraphic observation and age data was applied. Using the OxCal 4.2.3 program (Bronk Ramsey, 2013), we developed age models that use the radiocarbon dates from

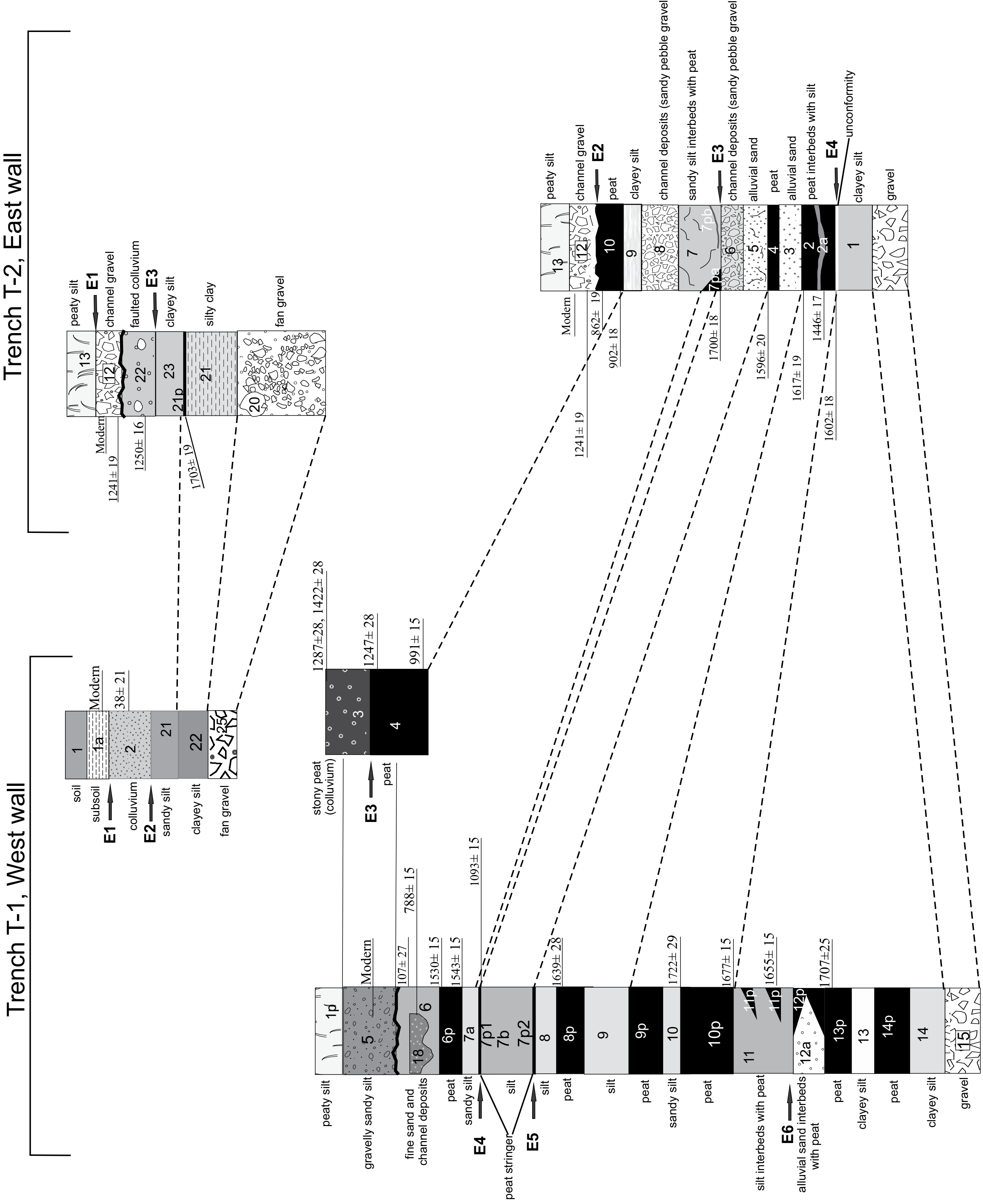

Figure 7. Simplified stratigraphy and age of the units from Hope Shelter site trenches. Arrows point to earthquake event horizons described within the text, and dashed lines correlate units based on stratigraphic, textural, and chronologic grounds. Calibrated radiocarbon ages (yr B.P.) of the units are attached to the columns. See Appendix 2 for complete unit descriptions.

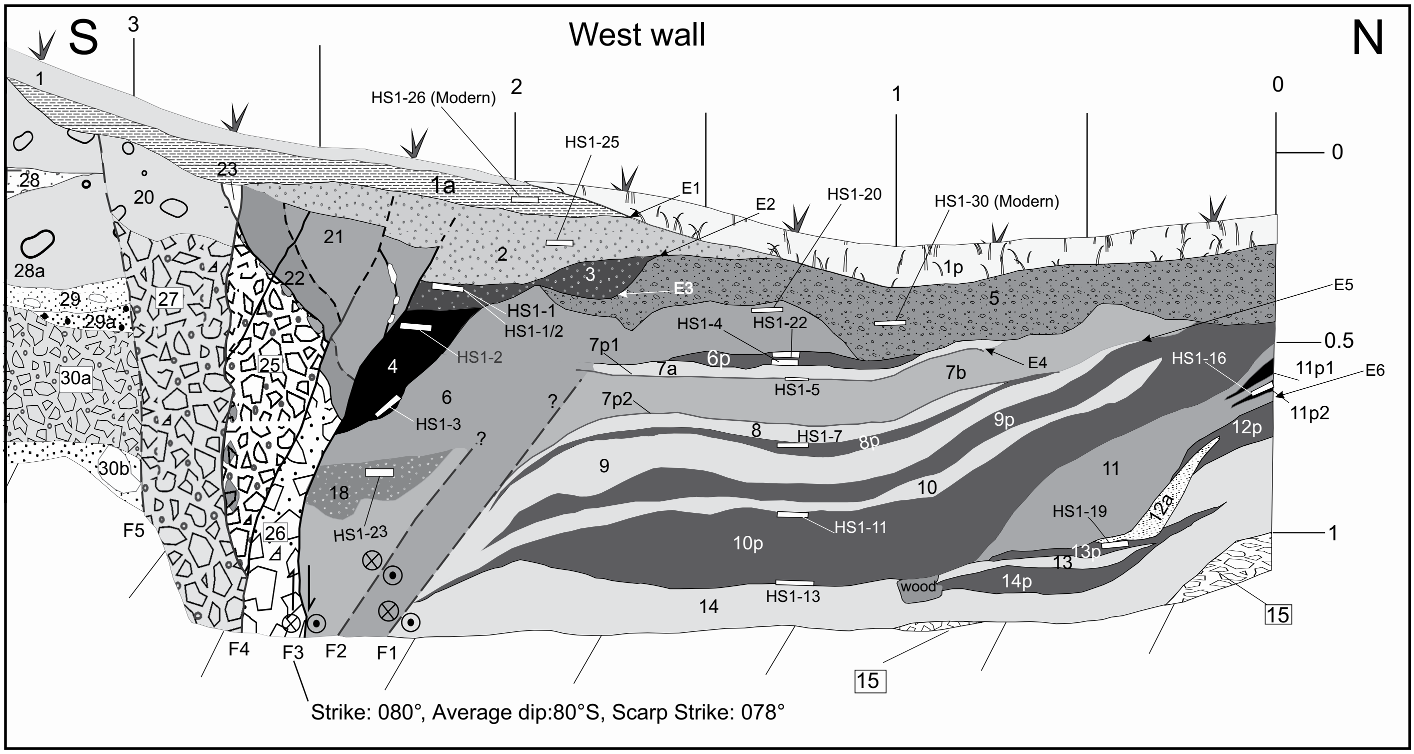

Figure 8. The first 3 m of trench T-1 are shown in detail. Trench wall was logged at a scale of 1:10. Sample locations and names are included. Black units represent peat, and gray units represent silt; see Appendix 2 for unit descriptions. Faults are shown in solid lines where certain, and dashed lines where uncertain. Fault F3 is identified as the main fault based on its position in the trench; i.e., it juxtaposes the fan deposits against the swamp deposits.

the paleoseismic trenches, along with dendrochronological and historical age constraints, in a Bayesian framework (e.g., Biasi and Weldon, 1994; Biasi et al., 2002; Howarth et al., 2014). Bayesian sequence statistics can systematically reduce the age uncertainty of individual and collective dates and event distributions (Scharer et al., 2007; Langridge et al., 2013). In this study, the two trench walls were independently modeled to avoid any error resulting from miscorrelating the horizons.

RESULTS

Geomorphic Descriptions of the Hope Shelter Site

The results of geomorphic analysis at the Hope Shelter site are presented here. Important surfaces and deposits around the Hope Shelter site include: (1) a faulted Holocene terrace (17 m above the modern Hope River); (2) a faulted low-gradient Holocene fan (herein called the shutter ridge fan) that emanates from a range-front catchment and grades to the terrace; (3) another faulted Holocene fan (herein called the Hope Shelter fan) at the west of the site that overlies the terrace and has preserved a cumulative dextral displacement; (4) a channel, and a shutter basin that formed behind the shutter scarp on the surfaces of the Hope Shelter fan and the shutter ridge fan, which we interpret as a deeply incised channel related to a small hot spring that is of no use in assessing discrete displacement; and (5) a faulted debris deposit at the middle of the site that overlies the shutter ridge fan and part of the shutter basin (Figs. 4A–4B). During dry months, peat accumulation occurs over the entire swamp floor; however, during wetter periods, sands and silts are deposited in the middle of the swamp, preventing peat accumulation there, but near the swamp edges, peat accumulation continues.

Structural Description of the Hope Shelter Site

The Hope fault at the Hope Shelter site is structurally simpler compared to the adjacent areas. A fault trace with a strike of 075° is clearly visible on aerial photographs, on the ground, and on the LiDAR hillshade model. It is characterized by an uphill-facing scarp that forms a shutter ridge with variable height (0.2 m to 1.5 m). A single trace of the fault cuts the Hope Shelter and shutter ridge fans, and the debris deposits, and splays/bends off toward the east (near Boundary Stream) and then ascends a postglacial alluvial fan (Fig. 3). On the postglacial alluvial fan, the fault appears as a series of en echelon uphill-facing scarps (0.2 to ~14 m high; see also Khajavi et al., 2014).

Fault Slip Measurement at the Hope Shelter Site

Series of dextral displacements were measured at this site between a large stream to the west (herein called Hope Shelter Stream; Figs. 2 and 4A) and Boundary Stream to the east in order to understand the slip pattern at the Hope Shelter site. These field measurements from west to east are 10 ± 1 m, 14 ± 3 m, 2.6 ± 0.3 m, and 4.6 ± 0.5 m, located in the vicinity of the trench site. From west to east, the 10 ± 1 m displacement was measured along a displaced gravitational failure scarp, the 14 ± 3 m displacement was measured along the displaced toe of the Hope Shelter fan adjacent to the Hope Shelter hut, the 2.6 ± 0.3 m displacement was measured along the edge of the debris deposit near the trenches, and the 4.6 ± 0.5 m displacement was measured along an abandoned channel on the terrace surface (Fig. 4A). The cumulative displacement of

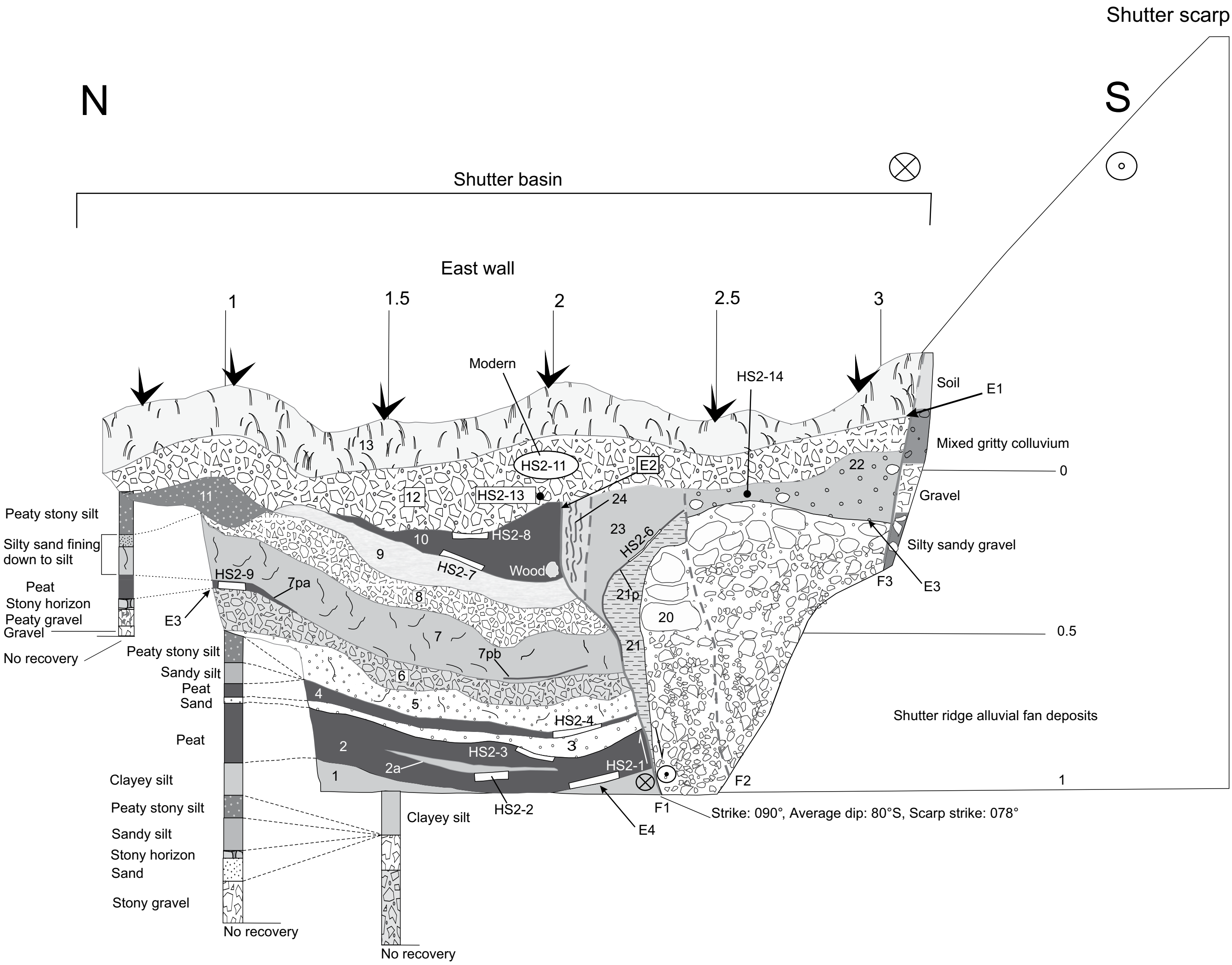

Figure 9. Trench T-2 and augur locations. Trench wall was logged at a scale of 1:10. Observations of the back wall of T-2 are described at the right side of the figure. Black units represent peat, and gray units represent silt; see Appendix 2 for unit descriptions. Faults are shown in solid lines where certain, and dashed lines where uncertain. Fault F1 is identified as the main fault based on its position in the trench; i.e., it cut units 1–10 and developed a considerable shear zone. See Appendix 2 for unit descriptions.

the Hope Shelter fan is considered to be the only reliable data for estimating the slip rate. The smallest measured displacement is consistent with the highest displacement (2.6 m) measured by McKay (1890) following the 1888 event, and with the average single-event displacement (3.4 m) measured by Langridge and Berryman (2005) at the McKenzie fan site, and with the single-event displacement (3 ± 0.4 m) measured by Khajavi (2015) at Matagouri Flat along the western Hurunui segment (Fig. 2). However, the 2.6 ± 0.3 m displacement at the Hope Shelter site is quite a bit smaller than the single-event displacement (4.5 ± 0.6 m) measured by Langridge et al. (2013) at Matagouri Flat (Fig. 2).

Hope Shelter Trenches

A sharp stratigraphic contrast was observed in T-1 and T-2 between the shutter ridge and basin stratigraphy. The stratigraphy of the two trenches is summarized in Figure 7. To avoid confusion, fault zone stratigraphy has been separated from the basin stratigraphy. Only the west and east walls of T-1 and T-2 were logged, resulting in two mapped walls ~4 m apart. Both trenches have a similar stratigraphy characterized by (1) alluvial and colluvial gravels exposed in the shutter ridge/scarp; (2) a fault zone consisting mainly of gravels, sands, silts, and colluviums; and (3) shutter basin deposits that are mainly well-bedded sands and silts and peaty soils.

In addition to the two main trenches and pit 1, we dug three pits on the surface of the shutter ridge fan and terrace (Fig. 4). Pit 2 was not logged or sampled because there was no evidence of paleochannel deposits. Pit 3 showed evidence for a paleochannel. Pits 1 and 3 indicate that due to the evolution of the fault scarp, at least two channels have been abandoned on the fan surface to the west of the debris deposit. Pits 1 and 4 were used to date the fan and terrace surface. Logs of these pits are included in the Data Repository (see footnote 1).

Trench 1

Trench 1—Stratigraphy

The main focus of the trench was the basin section and its relationship with the main fault zone, exposed across the scarp (Figs. 6 and 8). The deposits in this part of the trench are dominated by peaty basin materials, fine clastic deposits, and scarp-derived colluvial deposits (Fig. 8). Detailed unit descriptions are provided in Appendix 2. Tie lines in Figure 7 were drawn on the basis of stratigraphic position, sequence stratigraphy, and chronologic correlations (i.e., age of the organic samples). In general, three variably deformed packages consisting of alternating peat and silt sequences were identifiable in T-1 from meters 0 to 2 (Fig. 8). The lowest package begins with gravel (unit 15) and ends with silty alluvium (unit 11; Figs. 7 and 8). The middle package begins with a thick peaty horizon that interfingers with three silt units and ends with silt (unit 8). The uppermost package begins with a thin peaty horizon (unit 7p2) that has a subtle angular unconformity with unit 8p and ends with a thicker peaty horizon (unit 6p). The upward extensions of these packages are overlain by a lower gravelly sandy silt (unit 5) and upper surficial peaty soil (unit 1p; Fig. 8). The southern extents (to the south of T-1) of the silt-peat sequences seen in the middle package of the trench are highly deformed and are juxtaposed against unit 6, a massive, structureless silt deposit. The southern extents of the silt-peat sequences in the uppermost package are less deformed, with an upward-decreasing deformation pattern. Subtle deformation occurs in the northern extensions of the upper horizons (unit 7p1, 7a, and 6p) in the uppermost package.

Seventeen samples (mainly peat) were radiocarbon dated from T-1 (Table 2). More than half of these dates were in stratigraphic order and are considered to be valid in situ ages. However, several other samples, particularly within and overlying the fault zone, were either out of order, in reverse stratigraphic order, or of modern age, making their relevance and interpretation difficult. These dates highlight issues in sampling and assessing multi-event records from strike-slip faults.

Eight peat samples from the lowest three packages were radiocarbon dated (Figs. 7 and 8; Table 2). Faulted alluvium (units 6 and 18), faulted gritty peat (unit 4), and sandy to pebbly peat (unit 3) were observed between the deformed packages and the main zone of faulting. The upper boundary of unit 6 was marked by an erosional unconformity (Figs. 7–8). Five radiocarbon samples within these units were dated (Figs. 7 and 8; Table 2), and later we dated another piece of wood from sample HS1-1 (sample HS1-1/2; Table 2) to test the reliability of the reverse order of ages from unit 18 to unit 3. Within the fault zone stratigraphy (Fig. 7), the faulted basin units 21 and 22 are juxtaposed against units 3 and 4. These are the southernmost basin units on the log (Fig. 8). Units 3 and 21 are overlain by colluvium and soil (units 2, 1a, and 1; Fig. 7). The base of the colluvium, which we interpret as being scarp derived, has been faulted, while its top is truncated and overlain by more recent material. Two radiocarbon samples from units 2 and 1a were dated, but one was modern in age (Figs. 7–8; Table 2). To the south of T-1, from meters ~3 to 4.6 (Fig. 6), faulted fan gravels (units 25, 26, 27, 28, 28a, 30a, and 30b), faulted sandy channel deposits (units 29, 29a), and faulted scarp-derived colluviums (units 20 and 23; Figs. 6 and 8) are prevalent.

Trench 1—Faulting

The entire zone of faulting in T-1 extends across the width of the scarp for ~3 m, whereas the zone of most recent faulting spans only 1–1.5 m (Fig. 8). The main zone of faulting includes several vertical and subvertical shears F1–F5 (Fig. 8). The secondary faults F6 and F7 occur ~1–1.5 m south of the main fault zone at meters 4–5 (Fig. 6). Fault F3 in T-1 has a strike of 080° and an average dip of 80°S. On the surface, the fault scarp strikes 078°, as measured in the field, and 075° as measured on the LiDAR hillshade model.

The most recent faulting event (E1) in T-1 was identified by the upward termination of faults F3 and F4 at or above the base of unit 2, defined as a colluvial wedge. The unit 2 colluvium is likely faulted; alternatively, this colluvium is draped across the tips of faults F3 and F4. Unit 1a (subsoil) postdates the most recent faulting event (Fig. 8). Sample HS1-26 from unit 1a yielded a modern radiocarbon age. Seeds within unit 2 (sample HS1-25) should be older than, or of an equivalent age to, the deposition of colluvium indicating that E1 occurred at ca. 1817–1921 C.E. Given the reported age distribution, we cautiously attribute E1 to the 1888 Amuri earthquake.

Faulting event 2 (E2) was identified by the deposition of the colluvial unit 2 and faulting of the peaty colluvial unit 3 (Fig. 8). Sample HS1-25 (seeds) from unit 2 could either be older, or equal to, E2 in age, because it was deposited in the colluvial unit 2. The E2 event is undoubtedly older than the 1888 event. Therefore, E2 is likely to be older than 1840 (i.e., predating the colonial [historical] period in New Zealand). We dated samples HS1-1 and HS1/2 from unit 3 because the ages of these samples should predate the age of E2 and mark the earliest age for it. The calibrated ages of the samples were between ca. 600 C.E. and ca. 900 C.E. These samples are substantially older than sample HS1-25 and are in the reverse order to samples HS1-2, HS1-3, and HS1-18. This results in three possible interpretations: (1) Unit 4 has been vertically transferred up to this level; (2) units 3 and 4 have been rotated, and the materials dated were originally deposited at the base of these units; or (3) dated materials have been reworked and are thus older than their hosting sediment. Based on the results from T-2, we think that samples HS1-1 and HS1-2 are reworked materials, but sample HS1-3 could be the most reliable sample because its age is similar to the ages of samples HS2-7 and HS2-8 from peat unit 10 in T-2. Therefore, we favor option 3 (Table 2; Figs. 7–9).

Faulting event 3 (E3) was identified by faulting of peat unit 4 and deposition of peaty colluvial unit 3 (Fig. 8). Sample HS1-3 predates the event, and sample HS1-25 postdates the event; therefore, E3 is bracketed between ca. 1034 C.E. and 1817 C.E. This interpretation is based on accepting the age of sample HS1-3 as the correct age.

Faulting event 4 (E4) was identified based on the subtle deformation of units 7p1, 7a, and 6p from the uppermost deformed package (Fig. 8). Samples HS1-22, HS1-4, and HS1-5 were dated from this package. Samples HS1-22 and HS1-4 from unit 6p have an age overlap and indicate that the peat mean accumulation rate is ~0.5 mm/yr. Sample HS1-5, which comes from a rooty peat stringer, has a much younger age than sample HS1-4. This suggests contamination by roots from plants growing on the upper units. Therefore, we interpret that sample HS1-22 postdates this event, and sample HS1-3 predates this event: Event 4 is bracketed between ca. 554 C.E. and 1151 C.E. The fault that caused this event is shown as a dashed fault on the trench log based on the juxtaposition of the three deformed packages of silt-peat sequences against alluvial unit 6, and the progressive deformation of the three packages toward this contact (Fig. 8). However, no clear fault contact was observed at that location.

Faulting event 5 (E5) was identified based on folding that caused the slight angular unconformity where unit 7b drapes over units 7p2–9 (i.e., between the middle and the uppermost deformed packages; Fig. 8). This event should be younger than sample HS1-7 from peat unit 8 and older than sample HS1-4 from peat unit 6p. The event date is bracketed between ca. 412 C.E. and 627 C.E.

Faulting event 6 (E6) was identified between the middle and lowest deformed packages. The event horizon is unclear, but it is most likely to

TABLE 2. RADIOCARBON DATING RESULTS FROM THE HOPE SHELTER TRENCHES, WESTERN HOPE FAULT

Sample ID	Lab number	$\Delta^{13}C$ (‰)	Radiocarbon age (yr B.P.)	Calibrated age (2σ) C.E.				Probability for each 2σ range (%)				Sample type and description
Hope Shelter trench 1, C-14 samples, February 2012												
HS1-1	NZA 40297	–29.6	1287 ± 15	694–749	765–874			29.5	65.5			Peat: degraded plant material
HS1-1/2	NZA 51111	–27.7	1422 ± 28	609–692	750–763			92.8	2.4			Peat: degraded wood or bark
HS1-2	NZA 51108	–28.1	1247 ± 28	721–741	770–898	922–942		2.9	88.7	3.3		Peat: single woody stalk
HS1-3	NZA 40300	–27.2	991 ± 15	1034–1151				94.8				Peat: twig bark fragment
HS1-4	NZA 40305	–27.1	1543 ± 15	543–627				94.6				Peat: lump of plant tissue/bark
HS1-5	NZA 40302	–30.1	1093 ± 15	987–1023				94.7				Peat: root fragment
HS1-7	NZA 51110	–29.6	1639 ± 28	412–549				94.9				Peat: bulk sample of 12 peat lumps
HS1-11	NZA 51112	–27.9	1722 ± 29	257–302	317–436	491–508	520–527	10.5	82.2	1.7	0.6	Peat: 5 small lumps plus a small amount of peaty fragments (treated as bulk)
HS1-13	NZA 40299	–27.9	1677 ± 15	390–534				94.8				Peat: slender wood fragment
HS1-16	NZA 40298	–29.4	1655 ± 15	415–536								Peat: a seed, a short thin twig, and three small bark fragments (treated as bulk)
HS1-19	NZA 40317	–26.7	1707 ± 25	262–280	327–461	484–532		3	83.8	8.4		Peat: six seeds
HS1-20	NZA 51109	–24.4	107 ± 27	1698–1725	1808–1949			12.3	82.8			Bulk sample of sand: single peaty Raupo root
HS1-22	NZA 40244	–28.6	1530 ± 15	554–639				94.9				Peat: wood fragments
HS1-23	NZA 40245	–28.7	788 ± 15	1229–1251	1261–1290			17.7	77.8			Colluvium: Orangey brown flaky plant tissues
HS1-25	NZA 51076	–27.4	38 ± 21	1817–1829	1893–1921			42.6	52.4			Colluvium: four whole seeds and ~6 small seed fragments and two plant materials (treated as bulk)
HS1-26	NZA 51107	–29.4	Modern									Bulk sample of soil: stalky plant fragment
HS1-30	NZA 57002	–28.2	Modern									Bulk sample of alluvium: small plant fragments (flower head, grass, 5 blades, etc.)
Hope Shelter trench 2, C-14 samples, February 2013												
HS2-1	NZA 56458	–28 ± 0.2	1602 ± 18	428–548	561–570			92.2	2.7			Peat: stalky plant material
HS2-2	NZA 53421	–29 ± 0.2	1446 ± 17	613–667				95				Peat: twig
HS2-3	NZA54169	–27.5 ± 0.2	1617 ± 19	428–555				94.8				Peat: seeds
HS2-4	NZA 53410	–37.9 ± 2	1596 ± 20	431–580				95				Peat: woody plant material (twigs/stems)
HS2-6	NZA 53411	–34.4 ± 2	1703 ± 19	226–274	334–440	486–531		0.9	86.8	7.3		Peat: seeds
HS2-7	NZA 53416	–30.7 ± 2	902 ± 18	1158–1220				94.8				Peat: seeds
HS2-8	NZA 53412	–34.9 ± 2	862 ± 19	1187–1268				95.4				Peat: seeds
HS2-9	NZA 53414	–31.9 ± 2	1700 ± 18	337–442	453–460	485–531		85.6	0.7	8.8		Peat: two small lumps of peat
HS2-11	NZA 53386	–30.7 ± 0.2	Modern									Bulk sample of channel/colluvium?: a leafy fragment
HS2-13	NZA54166	–25.8 ± 0.2	1241 ± 19	776–895				94.8				Bark of a piece of dark-brown wood
HS2-14	NZA 53384	–32 ± 2	1250 ± 16	777–888				95.4				Bulk sample of colluvium: a leafy-looking fragment

be between units 10p and 11 or between units 11 and 12–13 (Fig. 8). If we restore unit 11 to its horizontal position, it appears that its upper contact with peat unit 10p is convex in shape. In cross section, units 11 and 12a have the form of a (tilted) paleochannel with interfingered peat, similar to what can be seen accumulating in the shutter basin today. Because the upper boundary of unit 11 includes clean silt that is slightly peaty, and unit 10p is the thickest peat unit in T-1, we infer that there was slow transition from an alluvial environment to a peatier environment (see units 11 and 10p descriptions in Appendix 2). This observation weakens the hypothesis of the event horizon being between units 10p and 11. However, the lower boundary of unit 11, which includes gritty silt with no evidence of peaty fibers, is most likely to be the event horizon. Taking that into account, the event horizon is constrained between sample HS1-19 from unit 13p and sample HS1-13 from unit 10p (Fig. 8), i.e., the event date is bracketed between ca. 262 C.E. and 534 C.E.

Trench 2

Trench 2—Stratigraphy

The stratigraphy in T-2 is consistent with our observations at the surface of the shutter ridge and basin and in T-1, showing that basin sediments were deposited or juxtaposed against the fan gravels derived from the shutter scarp. Detailed unit descriptions are provided in Appendix 2. The stratigraphy of T-2 is somewhat simpler than that of T-1 (Figs. 7 and 9) and comprises one deformed package of sediments. This package (units 1–10) consists of alternating peat, silt, sand, and gravel units that have been folded into a syncline and vertically dragged along fault F1 (Figs. 5 and 9). Units 1–10 are juxtaposed against fine-grained swampy deposits to the south of fault F1. Observations from the auger holes and the north edge of the trench imply that some of the marginal units in the basin have an interfingering relationship with the units within the deformed package (Fig. 9). Figure 7 also indicates the possible unit correlations between the two trenches, based on the grain size, relative elevation, and age of those deposits in T-1 and T-2. Differences in the actual elevations of these units can be explained by the possible existence of unconformities, considering the slope (to the west), and likely deformation of units within the basin, especially considering the observed warping adjacent to the fault zone (Figs. 8 and 9). Taking into account the results of the auguring, dating, and unit descriptions, we think that units 1, 2, 3, 7, 10, 20, 21, 23, and 13 in T-2 are equivalent to units 14, 10p, 9, 7, 4, 25, 22, 21, and 1p in T-1, respectively (Figs. 7–9).

Seven peat samples from the deformed package were dated (Figs. 7 and 9; Table 2). Within the fault zone stratigraphy (Fig. 7), the faulted fine-grained swampy units 24, 23, 21p, and 21 are juxtaposed against the deformed package to the north and against the fan gravels to the south. These units appear to be equivalent to the faulted (ponded?) units 21 and 22 in T-1. From unit 21p, sample HS2-6 (including 6 small seeds) yielded an age of 1703 ± 19 yr B.P. (Fig. 9; Table 2), which is equivalent in age to the basal units in both T-1 and T-2. These observations allow us to speculate that the stratigraphy within the fault zone can be correlated between the two trenches and also used to estimate the relative vertical displacement across the fault since ca. 300 C.E. From unit 21 toward the southern end of T-2, faulted fan gravels (unit 20) and a colluvial wedge (unit 22) were identified. One organic sample (leaf fragment) from unit 22 (HS2-14) was radiocarbon dated at 1250 ± 16 yr B.P. (Fig. 9; Table 2). An erosional unconformity marks the upper boundary of units 11, 10, 24, and 23, which are all overlain by channel gravels and peaty soil (units 12 and 13; Fig. 9). Two organic samples (plant fragments) from unit 12 were dated; sample HS2-13 yielded a radiocarbon age of 1241 ± 19 yr B.P., but sample HS2-11 yielded a modern age (Fig. 9; Table 2). We concluded that neither of these two dates may reflect the true depositional age of unit 12.

Trench 2—Faulting

The zone of faulting exposed in T-2 is ~1.1 m wide and consists of shear fractures F1–F3 (Fig. 9). Fault F1 in T-2 has a strike of 090° and an average dip of 80°S, which are consistent with faults observed in T-1, and the fault scarp geomorphology. Fault F1 projects upward into an ~9-cm-wide zone of shearing (Fig. 9) within unit 24, which indicates the likelihood of multiple shearing events on this fault strand.

The most recent faulting event (E1) in T-2 was identified by the upward extension of the southernmost fault F3 at the base of the fault scarp, and faulting of the channel gravel (unit 12) and the peaty soil (unit 13?; Fig. 9). This event is the youngest in this trench. Because the ages of samples HS2-7 and HS2-8 are the youngest (ca. 1100–1200 C.E.), most reliable (derived from seeds), in correct stratigraphic order, and predate the age of E2 in T-1 (because they are equivalent to the age of sample HS1-3), we argue that the most recent faulting event is much younger than the age of sample HS2-8. We acknowledge that we have a poorer estimate of the age of the most recent faulting event in T-2 than we do at T-1.

The penultimate faulting event (E2) was identified by the upward termination of faults F1 and F2, faulting of the top of peat unit 10, and faulting of colluvial unit 22 (Fig. 9). Units 1–10 appear to be folded or dragged equally (i.e., they have nearly the same shape and similar dragging style at their southern ends where they contact fault F1). This event must be younger than sample HS2-8 (ca. 1187–1268 C.E.). HS2-8 predates the event because unit 10 existed prior to faulting. Therefore, we are confident that at least two faulting events occurred subsequent to the date obtained for sample HS2-8, because unit 10 is capped by faulted unit 12.

Faulting event 3 (E3) was identified by deposition of colluvial unit 22 (Fig. 9) and the angular unconformity between units 7pa and 6. This event is bracketed between samples HS2-14 (ca. 777–888 C.E., unit 22) and HS2-8 (unit 10). We infer that delicate leaf material sampled from within unit 22 probably provides an age equivalent to the deposition of colluvial unit 22. Therefore, event 3 likely occurred around 777–888 C.E. Sample HS2-9 is not in order related to samples from lower horizons (may come from reworked materials), so was not used for the age estimation of E3.

Faulting event 4 (E4) was identified by comparing the position of the stone line within unit 21 in T-1 to the position of the thin peaty horizon (21p) within the faulted fine-grained deposits and the unconformity between units 1 and 2 in T-2 (Fig. 9). Unit 21 in T-1 includes an obvious line of stones adjacent to fault F3, which could be attributed to the oldest faulting event within both trenches. Figure 7 shows that unit 21 in T-1 correlates with unit 23 in T-2, implying that the stone line is probably just above the thin peaty horizon and at or just below the base of the T-2 in the shutter basin. Sample HS2-6 yielded an age of 226–531 C.E. As mentioned previously, this age is very similar to the age of basal units in both T-1 and T-2. However, there is ~0.5 m vertical distance between the position of HS2-6 from unit 21p and the basal units. Therefore, we interpret that the thin peat unit 21p has been faulted, folded, and displaced vertically. Supporting evidence for vertically displaced unit 21p is the grain size similarity (i.e., clayey silt) between units 21 and 23 and unit 1 (see Appendix 2). Therefore, we think that E4 should have occurred during or before the deposition of unit 1 (i.e., it is younger than the age of sample HS2-6). Sample HS2-1 from the base of unit 2 provides the minimum age for event E4. Therefore, E4 is bracketed between samples HS2-1 and HS2-6, i.e., 265–570 C.E.

Age of Surface Features

Age of the Holocene Terrace and Fan at the Hope Shelter Site

Two samples of sand and silt were dated from the shutter ridge fan and the terrace (17 m above the modern river) using OSL. Sample HS-2012-1-1 (Table 3; 23.9 ± 1.5 ka) was taken from the lower sandy unit 92 cm below the surface in pit 1 to estimate the age of the fan and shutter ridge (Fig. DR3 [see footnote 1]; Fig. 6). This sandy unit correlates with unit 30C on the west wall of T-1. Sample HS-2012-4-1 (Table 3; 16.4 ± 1.2 ka) was taken from a silty unit at a depth of 45 cm below the ground surface in pit 4 to estimate the age of the distal end of the fan/terrace (Fig. DR5 [see footnote 1]). Both samples yielded glacial or postglacial ages (i.e., ages that are consistent with the last cold climate period in New Zealand), not related to the valley-filling period characterized by the Holocene deposits. The OSL ages are more consistent with the ages of the highest-elevation postglacial fans (~90 m above the modern river) in this area (12–24 ka; Nathan et al., 2002).

The elevation of the terrace at the trench site, as part of a degradational suite of terraces within the middle Hope Valley, suggests that it is of mid-Holocene age. To assess the age of the terrace, we developed a river downcutting curve for the Hope River valley following the methodology of Cowan (1989). He used elevation and estimated radiocarbon ages of three terraces from the Manuka Creek area along the Hope River segment of the Hope fault (which were 145, 10–17, and 3–3.3 m above the Hope River) to derive an average downcutting rate of ~4.8 mm/yr (during the period 0–3500 yr B.P.), and ~15 mm/yr (during 12,000–3500 yr B.P.). Here, in addition to his radiocarbon ages, we included a dated terrace from near the Hope-Kiwi confluence

TABLE 3. RESULTS OF OPTICALLY STIMULATED LUMINESCENCE (OSL) SAMPLES FROM TRENCH 1 AND PIT 1 EXCAVATED ON THE LOW-GRADIENT HOLOCENE FAN AND THE HOPE SHELTER TERRACE

Sample ID	Lab number	a-value	D_e (Gy)	Dose rate (Gy/ka)	Age (ka)
Hope Shelter, OSL samples, February 2012					
HS-2012-1-1	WLL1046	0.06 ± 0.01	104.08 ± 4.48	4.35 ± 0.21	23.9 ± 1.5
HS-2012-4-1	WLL1037	0.06 ± 0.01	74.59 ± 4.28	4.55 ± 0.19	16.4 ± 1.2

(Langridge and Berryman, 2005) and applied the OSL dates from the Hope Shelter site to the highest-elevation postglacial fan above it, which is the source of deposits for the terrace and shutter ridge fan. We infer that the OSL results provide an accurate representation of the age of the postglacial fan (16–24 ka), rather than the surfaces at the trench site. Heights of the terraces/fan surface were measured from the local river bed. From these data, we developed an average downcutting rate curve of ~4.2 mm/yr spanning the last ~16–24 k.y. (Fig. 10). Using this rate, we predict the age of the terrace below the shutter ridge (~17 m above the Hope River) to be ca. 3300 yr B.P. (+553, –360). The positive error bar (+553) is produced when we allocate the OSL age of 16.4 ± 1.2 ka to the highest-elevation fan, and the negative error bar (–360) is produced when we allocate the OSL age of 23.9 ± 1.5 ka to the highest-elevation fan. For simplicity, we only show the graph that allocates both OSL ages to the highest-elevation fan. If we eliminate the OSL ages from the graph, the same average age of ~3300 yr will be obtained for the terrace, as other data on the graph will still yield the same relation on Figure 10. This age is consistent with the oldest dates from the base of the shutter basin, and it is considerably younger than the OSL dates from both T-1 and pit 4. These results confirm that surfaces low in the valley are likely to be of mid- to late Holocene age. As the fan at the trench site gently grades to the Hope Shelter terrace, we believe that it probably has an age equivalent to the minimum age of the terrace. However, the minimum age of the fan is ~1700 yr, based on the radiocarbon age of the base of the swamp formed on its surface.

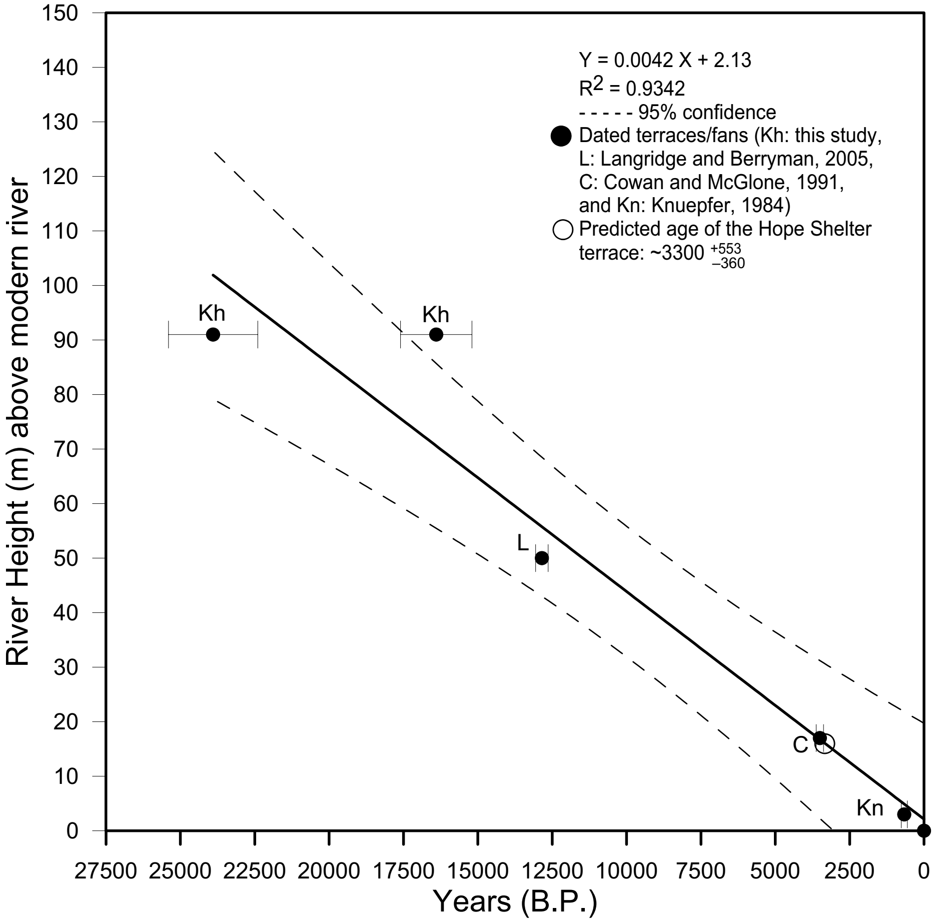

Figure 10. Hope River downcutting curve for the Hope River Valley. Age of the Hope Shelter terrace was estimated using the curve.

The older-than-expected OSL age results may be explained by insufficient bleaching during the remobilization of the sediment into the Holocene terrace and fan from the highest-elevation postglacial fan or insufficient transport and resetting down valley. This is not surprising given that rapid sediment remobilization and redeposition of sediments may be common in this environment. Such high rates and lack of bleaching conditions may arise because of rapid fan instability triggered by seismic activity or flooding, and short transport distances down valley, meaning that remobilization and redeposition may occur entirely within the darkness of a single night.

Age of the Debris Deposit at the Hope Shelter Site

At the trench site, the debris deposit overlies the middle part of the Holocene shutter ridge fan and the eastern part of the shutter basin (Fig. 4). It is composed of large angular boulders and is colonized by beech forest toward its head and Matagouri bushes toward its toe. A linear trough near the toe of the debris deposit, where the boulder clasts have been reorganized, indicates that it is faulted. A dextral offset of 2.6 ± 0.3 m is preserved at the western edge of the debris deposit. Therefore, an age assessment of the debris deposit and the timing of displacement was required.

A Schmidt hammer was used to compare the relative ages of the Hope Shelter debris deposit and a pre-1888 debris deposit near the Hope-Kiwi confluence (see Fig. DR6 and Part 4 of the Data Repository material [see footnote 1]). More than 70 boulders were sampled within each debris deposit. The mean values of the Schmidt hammer from the two deposits were compared using one-way analysis of variance (ANOVA; see Table DR1 [see footnote 1]). The results of ANOVA imply no significant age difference between the two groups. This suggests that the debris deposit at the Hope Shelter site was not generated during the 1888 event.

Dendrochronology was used to estimate the minimum age of the debris deposit. Sixteen red beech (*Nothofagus fusca*) trees growing on the debris deposit were cored and measured in 2012 using standard dendrochronological techniques, making notes of the growing condition and potential damage within the forest structure (for tree locations, see Fig. 4B). Trees were cored at the borer height (sternum height of the sampler) of 120 cm. Upon extraction, the cores were stored in plastic tubes (diameter: 7 mm). Following transportation, samples were glued and placed on core mounts; wooden blocks (45 × 4 × 1.7 cm thick) with two grooves in the middle (each groove ~6 mm wide and ~3 mm deep). The samples were sanded down to near their cross sections where we could see the rings. Ten of the tree cores contained all or some of the central rings of the trees and provided accurate dendrochronological ages (see Langridge et al., 2007). Six of the tree cores were shorter than the radius of the trees, providing minimum ages. Accurate ages were plotted against the tree diameter at the borer height (DBH) to produce the growth rate curve (Fig. 11A). We interpolated the minimum ages on the curve according to their DBH data (Fig. 11A). Age uncertainties associated with the interpolated data are shown as error bars with respect to the line of confidence. An age-frequency histogram was produced, with accurate and interpolated ages, using a 10 yr bin size (Fig. 11B). The age-frequency histogram shows a minor peak at ~110 ± 10 yr and a major peak at 130 ± 10 yr. Three trees with interpolated ages affect the gray bars of the histogram adjacent to the 1888 C.E. event (Figs. 11A–11B). One of the interpolated ages falls after 1888 C.E., one is included within the gray bar just before 1888 C.E., and one is included within the second gray bar before 1888 C.E. According to Figure 11A, these interpolated ages are associated with ±20 yr of uncertainty, meaning that they can shift or change the peaks, but at this stage, we cannot predict the exact effect of this on the histogram. However, if the ages of the three interpolated data are all overestimated or underestimated by ±20 yr, two peaks (pre- and post-1888) are still resolvable. Two trees give older ages: 197 yr (1815 C.E.) and 275 yr (1737 C.E.). The age of the oldest tree provides the minimum age for the debris deposit (i.e., 275 ± 10 yr). A distinct period of noncolonization (i.e., the period between 1815 and 1737 C.E.) appears on the histogram. The minor peak is consistent with forest recolonization immediately post-1888.

Apart from earthquakes, many processes, including fire, flood, hydrological change, wind, disease, and storm, can affect the structure of a forest. Perhaps the most obvious and visible effect in the modern forest is windthrow (uprooting and overthrowing of trees by the wind). We expect that windthrow is a significant background effect in the tree structure, which is evident by single tree colonization every few decades. We are confident that the Hope Shelter site was not deforested by fire at least since the European settlement, based on: (1) the absence of any historical report of deforestation at this site; (2) personal accounts of the land owners (pastoralists) that deforestation was unlikely at this site; (3) the absence of any trees that appear to be fire-damaged, in contrast with other sites affected by fire; and (4) the absence of charcoal within either of the trenches at the site.

We examined whether the 2.6 ± 0.3 m displacement of the edge of the debris deposit was from one or more than one event. The toe of the debris deposit occurs on the south side of the fault zone on the preexisting shutter scarp, and it has been faulted (Fig. 4). Therefore, it is younger than the preexisting shutter scarp and basin formed behind the fault scarp and is the youngest displaced geomorphic feature within the study site. The displacement recorded along the western edge of the debris deposit (2.6 ± 0.3 m) is consistent with the displacements measured by McKay (1890) following the 1888 Amuri earthquake (Fig. 2). This, in combination with the dendrochronology results, implies that the debris deposit could have been displaced once or twice since its deposition. If unit 12 (gravel) in T-2 comes from the reworking of finer-grained material associated with the debris deposit, then the maximum age of the debris deposit would be more than 275 yr but less than ~800 yr, because unit 12 is younger than ca. 800 yr B.P. (i.e., younger than sample HS2-8).

Age of the Surfaces near Parakeet Stream

Alluvial surfaces high in the landscape near Parakeet Stream (~800 m above sea level), were mapped in detail from LiDAR (Khajavi et al., 2014) in order to assess the Holocene slip rate. These surfaces have been displaced dextrally along the Hope fault by several tens of meters (Khajavi, 2015). Series of augers and pits were undertaken to derive the ages of gravel deposition or the abandonment of clastic deposition in favor of peat, which commonly blankets this upland landscape. The stratigraphy of typically shallow (1 m) pits and deeper (1.5 m) augers was logged, and organic samples were collected from above and below clastic horizons within these swamps (Figs. DR9–10 [see footnote 1]). Five radiocarbon samples were dated (Table 4).

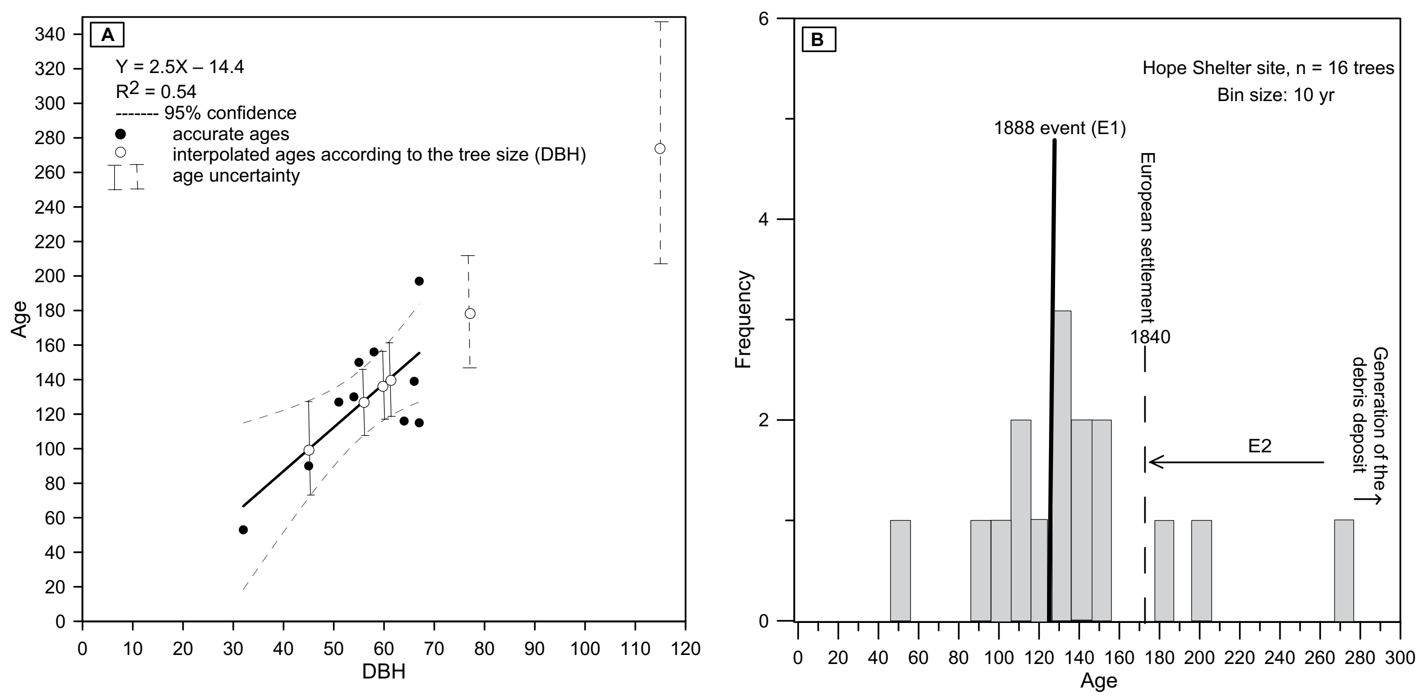

Figure 11. Results of the dendrochronologic study. DBH—diameter at the borer height. The 1888 event and historical period (C.E. 1840) are shown on the graph. (A) Graph showing a linear relationship between DBH and age of the trees. (B) Graph showing one major peak pre-1888 and one minor peak post-1888 using 10 yr bin size. Age is given in yr.

TABLE 4. RADIOCARBON DATING RESULTS FROM THE PARAKEET STREAM SITE, WESTERN HOPE FAULT

Sample ID	Lab number	$\Delta^{13}C$ (‰)	Radiocarbon age (yr B.P.)	Calibrated age (2σ) C.E.		Probability for each 2 σ range (%)		Sample type and description
Parakeet Stream: Pits, C14 samples, February 2013								
T3W-1	NZA 53427	–27 ± 0.2	395 ± 16	1460–1512	1548–1623	44.9	49.9	Peat: seeds
T3W-2	NZA 53430	–26.5 ± 0.2	380 ± 16	1479–1627		95.4		Colluvium: outer bark of a dark-brown twig
T4EP-4	NZA 54174	–28.9 ± 0.2	1624 ± 20	425–551		95.2		Peat: Peat lumps composed of plant tissues
T4WP-3	NZA 54160	–28.8 ± 0.2	903 ± 19	1156–1221		95.1		Peat: Wood pieces
OCWP-6	NZA 54154	–29 ± 2	2090 ± 21	113 B.C.E.–C.E.50	156 B.C.E.–134 B.C.E.	91.3	3.8	Peat: seeds

The ages of the samples were all considerably younger than the expected ages for those surfaces offset along the Hope fault, which would yield unreasonably high slip rates for the fault. Therefore, we reconsidered the stratigraphy and dates from Parakeet Stream in terms of a late Holocene record of off-fault landscape change processes (clastic earthquake-driven pulses overlying stable peaty upland surfaces) as proxies for the timing of surface faulting, rather than as estimates relating to larger cumulative displacements.

OxCal Modeling of Radiocarbon Ages

Using the OxCal 4.2.3 program (Bronk Ramsey 2013), two models were constructed for T-1 data (i.e., T-1 model 1 with six events and T-1 model 2 with five events). One model with four events for T-2 was constructed. The models included the historic 1888 Amuri earthquake, the beginning of the historical period (1840 C.E.), and the maximum age of the trees grown on the debris deposit (275 ± 20 yr). Details of the OxCal models (i.e., dates, event horizons, and commands) are presented in Appendix 3. The results of modeling T-1 and T-2 data are presented in Figures 12, 13, and 14. Timing of the events, distribution of the average recurrence interval (RI), mean (μ), median of the average RI, and the minimum and maximum times between the ruptures were calculated by OxCal at the 2 sigma (2σ) level (Table 5).

DISCUSSION

Paleoearthquakes on the Hurunui Segment

The trench exposures at the Hope Shelter site and related data provide the longest record of paleoseismicity along the Hope fault (see Cowan and McGlone, 1991; Langridge et al., 2003; 2013), extending back to ca. 300 C.E (Fig. 15). However, the results from trenches excavated in close proximity (i.e., 4 m apart) highlight the challenges in paleoseismic interpretations and imply a different number of events expressed or preserved in trench walls. T-1 provides evidence for five to six faulting events during the last ~1700 yr, and T-2 provides evidence only for four faulting events during the same period (Table 5; Figs. 7–10 and 12–15). The timing of events in the T-1 models was calculated as ca. 373–419, 439–580, 596–1092, 1106–1736, and 1825–1888 C.E. A possible sixth event, shown in T-1 model 1, likely occurred at 1819–1848 C.E. The timing of events in the T-2 model was calculated as ca. 373–495, 819–1192, 1235–1730, and 1733–1888 C.E.

Missing Earthquake Events?

The correlations between events from T-1 to T-2 and the differences in the interpretations of these two records suggest that we are possibly missing two earthquake events in T-2. The age of event E2 in the T-2 model overlaps with the ages of event E2 in the T-1 model 2 and event E3 in the T-1 model 1. The age of event E3 in the T-2 model is nearly consistent with the ages of event E4 in the T-1 model 1 and event E3 in the T-1 model 2. The ages of the most recent events in the T-2 OxCal model and T-1 OxCal model 2 span the ages of the two youngest events in the T-1 OxCal model 1 (i.e., there likely is an extra upper event in the T-1 model 1; Figs. 7 and 15; Table 5). The age of the oldest event in the T-2 model also nearly spans the ages of the two oldest events in both T-1 models (i.e., there likely is an extra lower event in the T-1 models; Figs. 7 and 15).

The existence of the extra upper event in the T-1 model 1 (i.e., if we interpret the deposition and faulting of unit 2 as two events) suggests

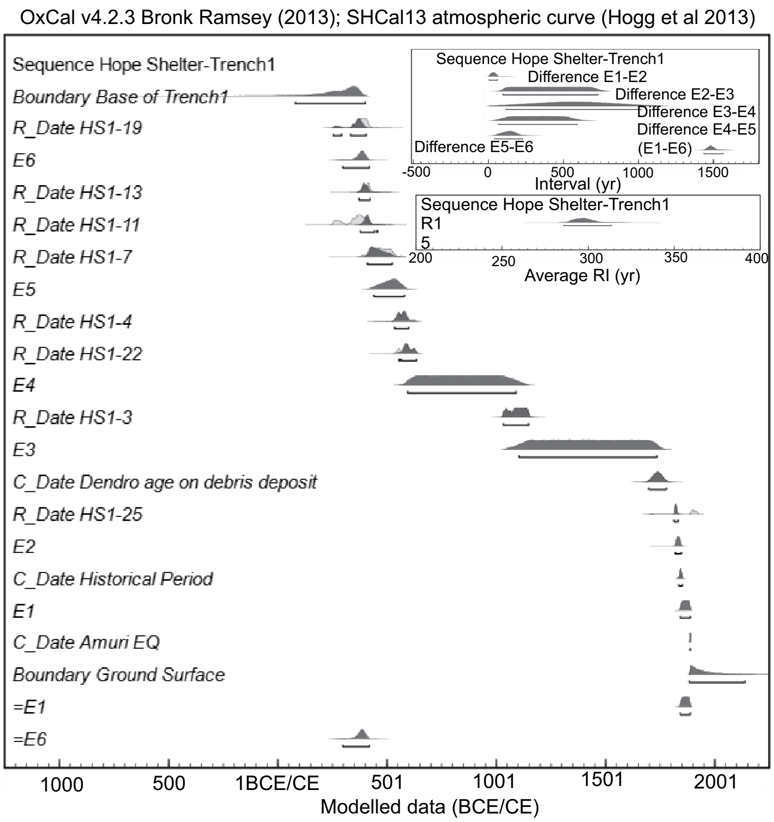

Figure 12. Results of OxCal modeling (trench 1 model 1) including date plots, plots of recurrence interval (RI) times between each two events, and average RI time. Calibration curved used for this analysis is SHCal13. E1–E6 are the earthquake (EQ) events.

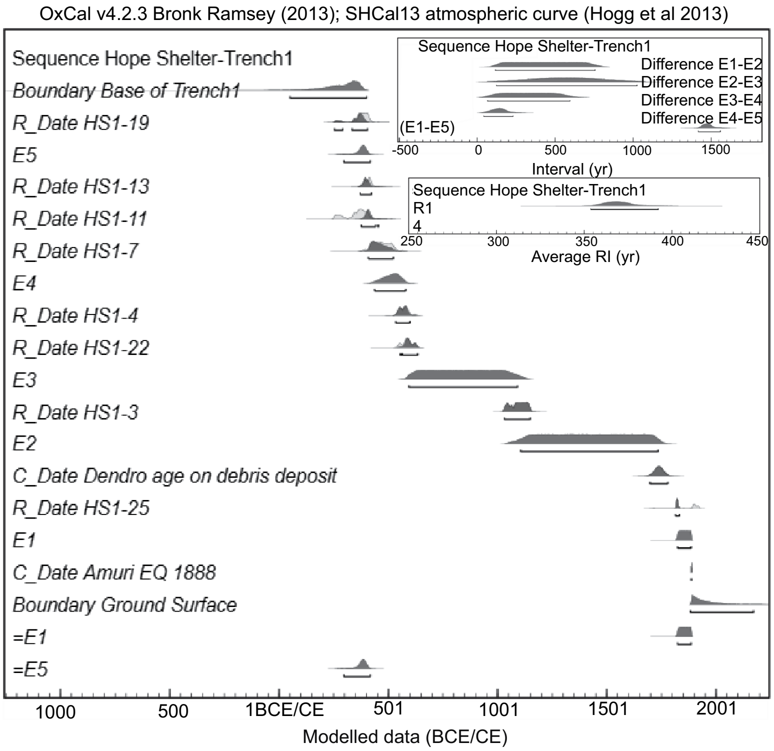

Figure 13. Results of OxCal modeling (trench 1 model 2) including date plots, plots of recurrence interval (RI) times between each two events, and average RI time. Calibration curved used for this analysis is SHCal13. E1–E5 are the earthquake (EQ) events.

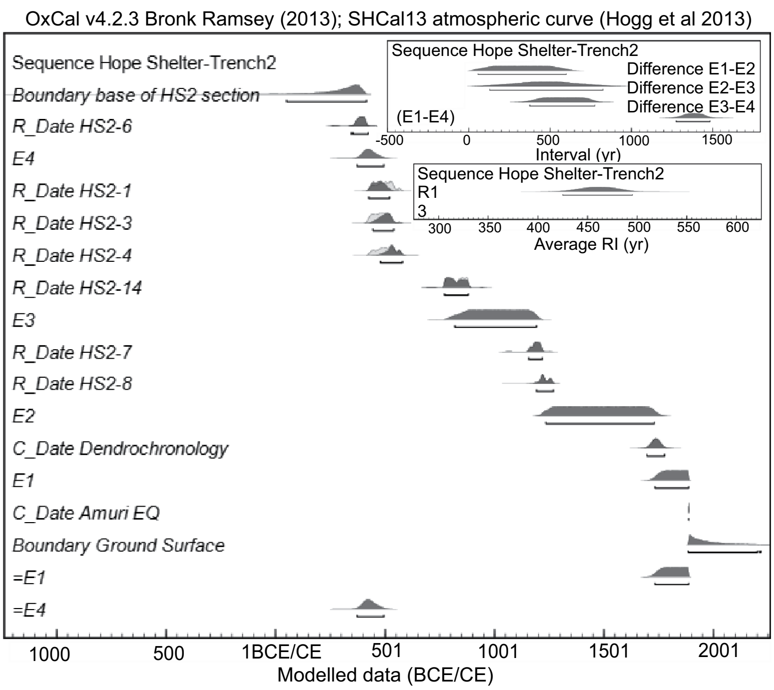

Figure 14. Results of OxCal modeling (trench 2) including date plots, plots of recurrence interval (RI) times between each two events, and average RI time. Calibration curved used for this analysis is SHCal13. E1–E4 are the earthquake (EQ) events.

that we are missing evidence for an event in T-2. We argue that fault F3 in T-2 could have ruptured twice recently, meaning that two events faulted unit 12. Our reason for this argument is that unit 12 could have been derived from the reworking of (i.e., postdates) the debris deposit on the surface. If this interpretation is valid, and the debris deposit has been faulted twice on the surface, the missing event in T-2 must have occurred on fault F3. Therefore, the two recent events in T-2 should be younger than ca. 800 B.P. (i.e., younger than our maximum age estimation of the faulted debris deposit using the age of sample HS2-8 in T-2).

A critical stratigraphic relationship within T-1 is whether unit 2 is a scarp-derived colluvium, and if it is, whether it has been subsequently faulted. According to the similarity between the ages of the penultimate events in the T-1 model 2 and T-2 model, it could be inferred that unit 2 in T-1 is unfaulted, and only draped across the fault scarp free faces immediately after the most recent event. If this interpretation is valid, we are not missing an event in T-2, but the age scenario of the debris deposit could remain valid. At this stage, both interpretations are possible; however, based on the age of unit 2 in T-1 and the only known historic event on the fault (the 1888 event), we favor the interpretation that unit 2 in T1 is faulted colluvium.

The existence of the extra lower event in the T-1 models suggests that we are missing evidence for another event in T-2. According to the stratigraphy of the trenches (Figs. 7–9), event E6 in the T-1 model 1 correlates well with the oldest event in the T-2 model. Therefore, we are missing an event between E3 and E4 in T-2. We argue that the missing event possibly occurred between units 4 and 5. This argument is supported by: (1) the chronology and position (Fig. 7) of the peat unit 4; (2) changes in the depositional environment (change from a quiet unit 4 peat to a more energetic alluvial environment unit 5 sand); and (3) the unconformity between units 4 and 5 to the north of T-2. Our interpretation, which relies on the changes in depositional environment as earthquake proxies, is consistent with the work of other researchers (e.g., Cowan and McGlone, 1991; Berryman et al., 2012; Clark et al., 2013).

Shaving of Paleoearthquake Ages

From the previous discussion, it can be inferred that we are missing two events in T-2, and our preferred record includes six events that occurred during the last ~1700 yr at the site (Fig. 15). Therefore, we give more credit to the T-1 model 1 than other models in terms of the number of the events. To construct our preferred model (i.e., the best possible unified

TABLE 5. PALEOSEISMIC HISTORY OF TRENCHES 1 AND 2 MODELED USING OXCAL PROGRAM

Events	Timing (C.E.)	The minimum and maximum times between every two events
Trench 1 (model1)		
E1	1843–1888	E1–E2: 5–60
E2	1819–1848	E2–E3: 97–729
E3	1106–1735	E3–E4: 118–1020
E4	596–1092	E4–E5: 65–595
E5	439–580	E5–E6: 41–230
E6	299–419	
Distribution of the average recurrence interval (RI): 285.7–313.7		
Mean: 297.968		
Median: 297.2		
Trench 1 (model 2)		
E1	1825–1887	E1–E2: 117–756
E2	1107–1736	E2–E3:122–1025
E3	596–1092	E3–E4: 66–595
E4	439–580	E4–E5: 42–231
E5	298–419	
Distribution of the average RI: 353.75–392.25		
Mean: 369.872		
Median: 368.75		
Trench 2		
E1	1733–1888	E1–E2: 58–600
E2	1235–1730	E2–E3: 128–825
E3	819–1192	E3–E4: 375–775
E4	373–495	
Distribution of the average RI: 424.833–495.333		
Mean: 460.705		
Median: 460.833		

Note: All of the values are reported at 2σ level. Two models are presented for trench 1 and compared with trench 2 model.

model in terms of the timing of the events), we examined the overlapping time between the events in the three models and the results of dendrochronology (see the event timings in our preferred model; Fig. 15). To examine the chronology of the events along the two segments of the Hope fault, we shaved the timing of the events in our preferred model considering all of the modeled events along the Hurunui and Hope River segments, including evidence for shaking events (Cowan and McGlone, 1991; Langridge and Berryman, 2005; Langridge et al., 2013) and the ages of the off-fault samples from augers and pits near Parakeet Stream (Fig. 15; Figs. DR9–DR10 [see footnote 1]). Taking that into account, the preferred timing and shaved timing of these six events were calculated as follows. The most recent faulting event correlates with the 1888 Amuri earthquake (1888 C.E.; Figs. 7, 11, and 15; Table 5). The penultimate faulting event (E2) likely occurred between ca. 1740 and 1840 C.E. An important constraint that we modeled for this event was that it had to have occurred before 1840 C.E., as there is no historical record of another large earthquake in the area between 1840 and 1888 C.E. The pre-penultimate faulting event (E3) possibly occurred between ca. 1479 and 1623 C.E. The faulting events E4, E5, and E6 likely occurred between 819 and 1092 C.E., between 439 and 551 C.E., and between 373 and 419 C.E., respectively.

Most Recent Faulting Event: The 1888 Amuri Earthquake

The combination of McKay's observations, our trench results, and other dating techniques provides strong evidence that the 1888 Amuri earthquake ruptured through the Hope Shelter site. Data from trenches provide support for at least one faulting event (E1) during the nineteenth century (1817–1921 C.E.; see age of the sample HS1-25), with an OxCal modeled age of 1843–1888 C.E. It appears that the most recent event faulted colluvial unit 2 in T-1, and this is consistent with evidence at T-2 (Figs. 7 and 9). We estimate a surface rupture length of 44–70 km for the 1888 Amuri earthquake. The minimum surface rupture length of 44 km is estimated from the Hope-Kiwi confluence (McKay, 1890), ~5 km west of our trench site, to the western margin of the Hanmer Basin (Cowan, 1991; Fig. 2B). The western extent of the 1888 rupture could have passed through the Parakeet Stream area, although no clear evidence for this was identified in our preliminary investigations. The maximum surface rupture length of 70 km is limited to the west by the trench site of Langridge et al. (2013), where dating appears to preclude the possibility that the 1888 Amuri earthquake ruptured this far to the west, with an easternmost trace location consistent with the maximum eastward position of rents and fissures observed east of the Hanmer Basin (Hossack Station; Fig. 2B; McKay, 1890). Conversion of surface rupture lengths to earthquake magnitudes using the scaling equation of Wesnousky (2008) yields an estimated magnitude M_w of 7.1 ± 0.1 for the Amuri earthquake.

The dendrochronology results (Fig. 11) provide several important insights applicable to the paleoseismic record: (1) The oldest tree sampled on the deposit had grown up to corer height by 1737 C.E., confirming that the emplacement of the debris deposit was not the result of the 1888 event; (2) the existence of a distinct period of noncolonization (1815–1737 C.E.) followed by the older major tree age peak at ~130 ± 10 yr clearly predates the 1888 event and could likely represent an earthquake that knocked down a group of trees before the European settlement of New Zealand (1840 C.E.); (3) the forest recolonization immediately post-1888 (Fig. 11; second peak at ~110 ± 10 yr) suggests that some trees could have been damaged or knocked down by the 1888 event, allowing younger trees to shoot up immediately following the 1888 event, as implied by McKay's observations of tree damage. Taken together, these results from dendrochronology collectively indicate that the debris deposit probably experienced two events in the last 275 yr (since 1737 C.E.), with some certainty that one of these events was the 1888 Amuri earthquake.

The results of this study confirm that the horizontal displacement of 2.6 ± 0.3 m measured at the western edge of the debris deposit at the Hope Shelter site is the result of one or two displacement events. Although a maximum coseismic displacement of 2.6 m in the 1888 Amuri earthquake was documented on the Hope River segment (McKay, 1890), the location of our study site closer to the end of the 1888 rupture extent, and on a different rupture segment, suggests that a smaller coseismic slip in this event is likely, which is consistent with the observation of decreasing surface rupture displacements toward rupture tips (e.g., Lin et al., 2012; Quigley et al., 2012). The base of the colluvial wedge (unit 2; Fig. 8) is interpreted as stepped, but it appears to be stratigraphically coherent across the fault zone; if larger (e.g., ≥0.5–1 m) coseismic displacement occurred, it is likely that this relatively thin (<20 cm) unit would have been structurally dismembered or juxtaposed against a different lithology.

Relationship between Surface and Subsurface Data and Slip Rate Estimation

From the relationship between the geomorphic features and their estimated ages at the Hope Shelter site, a horizontal slip rate can be computed. This study estimates the age of the shutter

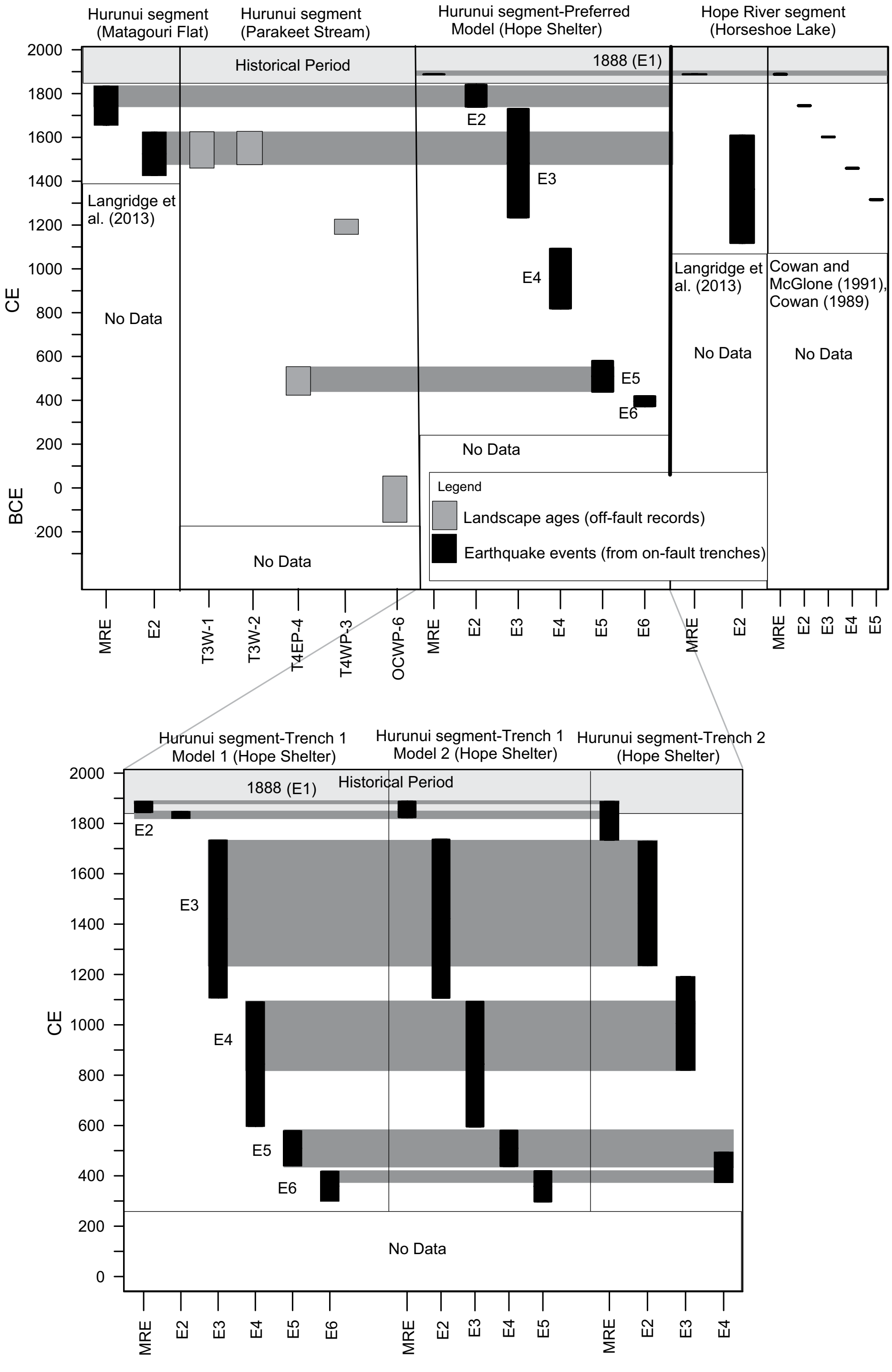

Figure 15. Timing of late Holocene paleoearthquake histories for the Hurunui and Hope River segments of the Hope fault including the 1888 Amuri earthquake. The events timings calculated by our models for the Hope Shelter site are presented and compared. Our preferred model for the Hope Shelter site represents six events, which were identified considering time overlaps between all of the available data for the two segments of the Hope fault. We compared two sets of data: (1) the on-fault trenching data, which are interpreted as direct evidence for surface faulting events (Cowan, 1989; Cowan and McGlone, 1991; Langridge et al., 2013; this study); and (2) the off-fault data (from pits on the swampy areas adjacent to and south of the fault scarp near Parakeet Stream), which are not direct evidence for surface-rupturing events. The bold vertical line on the top figure separates the Hope River segment data from the Hurunui segment data. MRE—most recent event.

ridge fan to be between ~1700 yr (based on the development of the shutter basin) and ~3300 yr (based on the estimated age of the Hope Shelter terrace according to the downcutting rate of the Hope River). The Hope Shelter fan has preserved a cumulative dextral displacement of 14 ± 3 m at the Hope Shelter site. This fan should probably have an equivalent age to the minimum age of the Hope Shelter terrace, because, like the shutter ridge fan, it also gently grades to the Hope Shelter terrace and has been entrenched by the shutter basin (Fig. 4). Therefore, using the minimum age of the shutter ridge fan (~1700 yr) and the 14 ± 3 m of cumulative displacement on the surface, we estimate a preliminary maximum horizontal slip rate of 6.5–10 mm/yr at the Hope Shelter site. This estimated slip rate is consistent with the estimated minimum horizontal slip rate of 8–11 mm/yr calculated for a site at the western part of the Hurunui segment (see Langridge and Berryman, 2005).

Earthquake Recurrence Interval

Using the Monte Carlo statistical approach, we calculated a mean recurrence interval (RI) of 298 ± 88 yr (see Part 7 of the Data Repository material [see footnote 1]) from preferred ages of the earthquake events (Fig. 15). This mean RI is consistent with the mean RI times calculated by the three individual OxCal models in this study (i.e., ~300, ~370, and ~460 yr; Table 5). The mean RI of 298 ± 88 yr overlaps with both previous estimates of RI = 310–490 yr for the Hurunui segment (Langridge and Berryman, 2005; Langridge et al., 2013) and RI = 81–200 yr for the Hope River segment (Cowan and McGlone, 1991). Cowan and McGlone (1991) proposed a periodic earthquake model for the Hope River segment (earthquake surface ruptures every ~81–200 yr); however, Langridge et al. (2013) interpreted that only two of the five events identified by Cowan and McGlone (1991) can be directly attributed to surface-rupturing events, and the rest could be attributed to shaking events that generated subsequent silt deposition in their trench on the Hope River segment (Table 1). Resolving this debate is beyond the scope of this study.

Periodic versus Episodic Earthquake Behavior

The faulted stratigraphy at the Hope Shelter site provides the longest and potentially most complete record of paleoearthquakes along the Hope fault, allowing for critical assessment of late Holocene earthquake behavior. Figure 15 shows a summary of event chronologies along the two segments of the Hope fault from which interevent times have been extracted. Based on the data from this study (Figs. 2 and 15), event E1 (1888) ruptured the Hope River segment and parts of the Hurunui segment, indicating that the western extent of the 1888 Amuri earthquake rupture is somewhere between the Hope-Kiwi confluence and Parakeet Stream, but not as far west as the Langridge et al. (2013) trench site. The most recent event of Langridge et al. (2013) provides support for the occurrence of an event (i.e., E2) ca. 1740–1840 C.E. on the Hurunui segment, which coincides with a strong shaking event along the Hope River segment (Langridge et al., 2013; Table 1). Based on the correlation between the Parakeet Stream data set and earthquake events, it appears that the stratigraphy in the Parakeet Stream sections represents seismically driven clastic pulses in a largely stable peat-forming setting associated with Hope fault earthquakes. This interpretation is strengthened by the radiocarbon dates, which are all of late Holocene age and typically separated by 300–500 yr across the Parakeet Stream area. The youngest dates at this site, which is located halfway between the Matagouri Flat and Hope Shelter trench sites (Langridge et al., 2013; this study), align with those at Hope Shelter, Matagouri Flat, and Horseshoe Lake (Cowan and McGlone, 1991). This provides support for the occurrence of an event (or events) between ca. 1400 and 1600 C.E. (i.e., E3) on both the Hope River and Hurunui segments (Fig. 15). One of the older dates (T4EP-4) at the Parakeet Stream site provides support for the occurrence of an event (i.e., E5) in the ca. 400–600 C.E. time frame on the Hurunui segment (Fig. 15).

Median interevent times between successive events identified from the Hope Shelter trenches range from 98 to 595 yr. Interevent times between E1 and E2, E2 and E3, and E5 and E6 are shorter than the mean RI, and median interevent time between events E3 and E4 and E4 and E5 are longer than the mean RI. There is a long average interevent time between events E4 and E3 (595 yr). It is our preferred hypothesis that E3 involved rupture of both the Hurunui and Hope River segments of the fault, either coseismically (and thus somewhat similar to the multisegment rupture in the 1888 Amuri earthquake) or in separate events spaced closely enough in time to be unresolvable from our dating resolution. A moderate average interevent time of ~239 yr exists between events E3 and E2, and a shorter average interevent time exists between events E2 and E1 (98 yr); the youngest event (E1, 1888) ruptured the entire Hope River segment and part of the Hurunui segment. There is a long interevent time of 460 yr between events E4 and E5 and a shorter average interevent time between events E5 and E6 (99 yr).

Interevent times that are significantly shorter than the mean recurrence interval can be explained by (1) coalescing rupture overlap from the adjacent Hope River fault segment onto the Hurunui segment at our study site (e.g., E1 and possibly E3), which could create apparent earthquake clustering irrespective of whether the individual segments exhibit periodic or episodic rupture behavior, and/or (2) earthquake temporal clustering (i.e., episodic temporal behavior) on the Hurunui and/or Hope River segments. Interevent times that are significantly longer than the mean RI can be explained by earthquake temporal clustering (episodic behavior), and/or "missing" or otherwise unresolved events (option 3). The final possibility (option 4) is that the apparently variable interevent times simply reflect limited chronologic resolution due to some large age ranges of radiocarbon samples. However, the large number of samples, use of OxCal modeling and different recurrence scenarios, and inability to fit periodic recurrence to the age data even with full consideration of age ranges suggest that option 4 is the least likely reason for the observed variability.

Given our conclusion that the 1888 Amuri earthquake involved coeval rupture of both the Hope River and part of the Hurunui segment, we consider rupture overlap (option 1) to provide a reasonable explanation for some of the temporal distribution of earthquakes at our study site, irrespective of whether individual segments exhibit periodic or episodic behavior. However, this scenario alone is unlikely to explain all of the observed variability, because some of the interevent times (i.e., E3-E4-E5) greatly exceed the proposed ranges of average interevent times on adjacent segments, particularly for the proposed periodic RI for the Hope River segment (Cowan and McGlone, 1991). Episodic rupture behavior on the Hurunui segment, Hope River segment, or both, could account for both the comparably short and long interevent times with respect to the mean RI. We cannot dismiss the possibility that we may be missing events from our trench record, despite the closely spaced and detailed nature of our investigations (option 3). "Missing events" could include earthquake ruptures that did not rupture through the trench site (i.e., ruptured other strands, or terminated beneath or outside of the trench extent), or those that did not leave a stratigraphic and structural record in the trench that was distinguishable from other events. Missing events could account for interevent times longer than expected from periodic recurrence intervals from the Hurunui and Hope River segments. With our current state of knowledge, we cannot easily assess the possibility that one or more events could have occurred but were not recognized during the time period encompassed by the trench stratigraphy. More paleoseismic studies along the Hurunui and Hope River segments of the Hope fault are required to refine the extent, timing, and rupture behavior of past earthquakes in this region.

Rupture Segmentation: Evidence for a Geometric Barrier between the Two Segments?

The preferred earthquake model for the Hope Shelter site indicates two events within the last ~250 yr and/or three events within the last 400–500 yr (Fig. 15). In contrast, the paleoseismic records from other segments along the Hope fault (Table 1) show evidence for two or three events within the last ~600–900 yr (Langridge et al., 2013). The discrepancy here can be explained by the location of our trenches, because they were excavated near a segment boundary, where the ruptures of the Hope River and Hurunui segments could overlap (e.g., events E1 and E2; Fig. 15). The boundary between the two segments is characterized by an ~850-m-wide right stepover in the fault associated with a 9°–14° fault bend (Fig. 3).

Several studies show that stepovers or bends separating fault segments can arrest or ease rupture propagation under certain circumstances (e.g., Barka and Kadinsky-Cade, 1988; Wesnousky, 2006, 2008; Oglesby, 2005; Elliott et al., 2009; Wesnousky and Biasi, 2011). In particular, studies on historical strike-slip surface ruptures (e.g., Wesnousky, 2006; Wesnousky and Biasi, 2011) have shown that stepovers ≥1 km are ~50% effective in stopping rupture propagation, while stepovers ≥3–4 km appear to arrest rupture propagation. Barka and Kadinsky-Cade (1988) also indicated that bend angles >30° may stop large rupture propagation. Other factors, such as the existence of structural complexity, or changes in the dynamic behavior of the rupture near the stepover, or the existence of fault segments separated by bends or stepovers with favorable orientations to rupture with respect to the regional stress field, can influence the rupture dynamics and propagation (Elliott et al., 2009).

According to the criteria explained by the previously cited studies, it seems that the conditions at the study site, between the two fault segments, are more favorable for rupture propagation than arrest. The width and bend angle of the right stepover between the Hope River and Hurunui segments are narrower and smaller compared to the rupture-limiting thresholds mentioned by the cited studies. In the overlapping area of the two segments just west of the bend, dextral slip has dropped dramatically, but transferred into vertical slip represented by a suite of en echelon structures (Khajavi et al., 2014; Fig. 3). Given characteristics such as the more favorable orientation of the Hurunui segment to rupture with respect to the regional stress field (Khajavi et al., 2014), the <1 km width of the local releasing stepover (e.g., Elliott et al., 2009; Wesnousky and Biasi, 2011), the rapid changes in the slip mode (dextral to vertical), and the comparable paleoseismic histories obtained from the trenches along both segments, it is likely that some of the ruptures can propagate through the bend and stepover and continue some distance along the adjacent segment (e.g., events E1 and E3; Fig. 15). Regarding event E3, we cannot confirm whether this event was a Hope River rupture that propagated toward the Hurunui segment, or vice versa, or a bilateral rupture. It appears that event E3 did not stop at the stepover and involved rupture on both segments, with a rupture length consistent with (or longer than?) the historical event E1 (the 1888 Amuri earthquake). Based on an oral account in McKay (1890), the 1888 rupture likely propagated from the west toward the east of Glynn Wye station (Fig. 2B; McKay, 1890; Cowan, 1991). Based on the results of this study, there are two possibilities: (1) The rupture could have nucleated on the Hurunui segment and propagated to the Hope River segment, via the bend and stepover, with a unilateral directivity toward the east; or (2) the rupture could have propagated bilaterally from Glynn Wye station (see Fig. 2; Appendix 1: 17) or from an unknown point west of Glynn Wye station. Because the Hurunui segment is better oriented for slip (Khajavi et al., 2014), it can be inferred that larger multisegment ruptures may be more likely to initiate on the Hurunui segment than on the Hope River segment. The possibility that rupture directivity and/or rupture velocity may have influenced whether Holocene ruptures propagated through or arrested near the study site remains a focus of future research. By demonstrating that the 1888 Amuri earthquake propagated through a proposed segment boundary, we provide the first evidence for coseismic multisegment ruptures on the Hope fault. In combination with our paleoearthquake chronology, we posit that earthquake recurrence along major strike-slip plate-boundary faults may vary between more periodic and more episodic end members, even on adjacent, geometrically defined segments.

CONCLUSIONS

Paleoseismic investigations of the Hurunui segment of the Hope fault coupled with reanalysis of historical observations (McKay, 1890) provide the first evidence for surface rupturing on this fault segment during the 1888 Amuri earthquake. The results of trenching, combined with construction of a slip gradient curve, show that the 1888 rupture could have had a surface rupture length of 44–70 km, and a magnitude of M_w = 7.1 ± 0.1. A preliminary maximum horizontal slip rate of 6.5–10 mm/yr was estimated at the Hope Shelter site on the Hurunui segment. The results from two closely spaced paleoseismic trenches excavated at the Hope Shelter site indicate that six earthquake events likely occurred in the past ~1700 yr. The timing (ca. C.E. 1888, 1740–1840, 1479–1623, 819–1092, 439–551, and 373–419) of these events was estimated using OxCal modeling and overlapping event times using data from our trenches, and other trenches along the Hurunui and Hope River segments, and the data from the Parakeet Stream site. A mean RI of 298 ± 88 yr was estimated for the identified events. Earthquake records on the Hurunui segment of the Hope fault contain evidence for short inter-event times (as short as ~98 yr) resulting from (1) rupture overlap and multisegment ruptures, and/or (2) earthquake temporal clustering, and/or (3) missing events. The geometrically defined segment boundary between the Hurunui and Hope River segments does not always act as barrier to rupture propagation, and analogous geometric discontinuities may not limit rupture dimensions elsewhere along the Hope fault, implying that the magnitude of future earthquakes may in some instances exceed estimates based on lengths of individual fault segments. This study highlights the possibility that paleoearthquake records near geometrically complex segment structural boundaries on major strike-slip faults may show temporal recurrence distributions resulting from earthquake ruptures that variably arrest or propagate through proposed segment boundaries.

APPENDIX 1. KEY OBSERVATIONS OF MCKAY (1890) AND JONES (1933) REGARDING THE 1888 NORTH CANTERBURY (AMURI) EARTHQUAKE

(1) "The distance of the Clarence accommodation-house (top right side of Fig. 2) from the line of greatest disturbance where it passes along the south side of the eastern part of the Hanmer Plain is some fourteen miles [22.5 km] in a north-north-easterly direction, but at a right angle from the eastern prolongation of the line it is not more than ten miles [16 km]." (McKay, 1890, p. 2)

(2) "…lake Sumner is ~6 miles [9.5 km] south of the earthquake-fracture at the junction of Kiwi Creek with the Hope River, and the lower part of the Otairo (Otira) Gorge not more than ten miles [16 km] south of the line as traced if continued westward." (McKay, 1890, p. 2)

(3) "Of the ground-rents said to have opened along the bed of the Percival River, these appear for the most part to have closed or been filled by the falling-in of

the sides, although Mr. Low of St. Helen's, informed me that he could still find one special rent open which was said to be nearly 10 in. [25 cm] in width. This, however, I did not see and in riding along the plain to the junction of the Hanmer with the Waiau-ua (Waiau River) I saw no fissures nor rents of any kind." (McKay, 1890, p. 4)

(4) "On our way through the Waiau-ua (Waiau) gorge Mr. Rutherford pointed out two slips on the east side of the gorge and stated that these had been caused by the earthquake of the 1st September…true fissures must be attendant, but they have not been observed." (McKay, 1890, p. 5)

(5) "At the bridge at the upper end of the gorge there were no visible signs of an earthquake having occurred, but I was told that some rocks had fallen on the Leslie Hills side of the river." (McKay, 1890, p. 5)

(6) "In following up the south bank of the Waiau-ua (Waiau River) not a trace of the effects of the earthquake was observed for the first four miles [6.4 km] west of the upper end of the gorge. At this distance, however, the track passes over a spur of the range on the south side of the plain…on the western face of the spur earth-rents that, when formed, might have been 4 in. [10 cm] or 5 in. [12.5 cm] wide, crossed the track in a westerly direction…" (McKay, 1890, p. 5)

(7) "Before reaching the crossing of the Waiau-ua (Waiau River) to Hopefield Station (Glenhope) the long cutting descending to the river-bed had been rendered almost impossible to horsemen…rents were everywhere on this cutting, some of them being more than 12 in. [30.5 cm] wide, and these, with the slipped outer edge of the road and fallen banks from the upper side, showed clearly that what the violence and force of the earthquake had been." (McKay, 1890, p. 6)

(8) "On the dray-road crossing from Hopefield (Glenhope) to the south bank of the river, just below the junction of the Hope, the road, going to Glenwye (Glynn Wye), crossing the broad low-sloping fan of Shingle Creek and on this rents and openings 4 in. [10 cm] to 6 in. [15 cm] in width began to appear and became more numerous as we proceeded westward. There were true fissures on a flat surface, unlike many that appeared on the edge of the terraces, where the ground rent was not equally supported on both sides." (McKay, 1890, p. 7)

(9) "…about half a mile east of Horse-shoe Lake a cubical mass of rock some 6 ft. [1.8 m] square encumbers the road. Seemingly it has fallen or rolled down from the heights above, but it had left no track in its passage to the lower ground…" (McKay, 1890, p. 7)

(10) " ....the higher terrace is 350 ft. [107 m] above the station flat (Glynn Wye Station), or nearly 500 ft. [152 m] above the river at the junction of Kakapo Brook…. …an old line of dislocation, caused by former earthquakes, runs along the middle of this higher terrace, and the recently-formed earth-rents follow the same course, or nearly so. At the back of the Glenwye (Glynn Wye) Station, the recently-formed fractures are on the face and brow of the high terrace, and a little to the west on the upper flat itself, where over nearly a quarter of a mile [0.5 km] the whole surface is a network of fractures, fissures, slips, and dislocations. At one place, an area of ~4 chains in width and 10 chains or more in length has subsided 2 ft. [0.6 m]… the middle part of this may have subsided even more than that. From Glenwye (Glynn Wye) Station, a wire fence…was shifted 5 ft. [1.5 m] out of the true line. About a mile and a half [2.4 km] beyond Glenwye (Glynn Wye) the fence…crosses the old earthquake-rent…has been sundered and thrown to the east a distance of 8 ft. 6 in. [2.6 m]. Less than a mile and a half [2.4 km] further west another fence…has been broken and shifted to the east 8 ft. [2.4 m]…as at the furthest west fence on the high terrace flat the amount of shifting was 8 ft. [2.4 m], and at Glenwye (Glynn Wye) Station 5 ft. [1.5 m], the movement cannot have begun and ended at these places. The displacement of the country to the north of the line of old fracture therefore probably extends from Hopefield (Glenhope) Station, at the junction of the Hope and Clarence (Waiau) to the junction of the Boyle with the Hope, a distance of 8 miles (13 km)…." (McKay, 1890, p. 9 and 10)

(11) "In the Hope Valley, above the junction of the Boyle River, the rents and fissures begin to be less abundant than they are in the vicinity of Glenwye (Glynn Wye)…." (McKay, 1890, p. 10)

(12) "A mile [1.6 km] below the junction of Kiwi we crossed from the south to the north side of the middle Hope Valley, we skirted the edge of the bush on the side, noting that very many of the dry birch-trees (beech trees) in the bush had been broken and thrown down by the earthquake, and that these were generally broken off 10 ft. [3 m] to 15 ft. [4.5 m] from the ground, the timber, though dry, being sound for the most part, and the roots holding firm in the ground…in other cases, green trees 25 ft. [7.6 m] to 30 ft. [9 m] in height have been torn up by the roots and are now in the prostrate position. This has happened both on shingly and on rocky soil." (McKay, 1890, p. 11 and 12)

(13) "We proceeded along the upper Hope Valley to Jones hut, which was reported to have been wrecked by the earthquakes of the 1st September, and near which report had it that a fissure had opened and again closed with such violence that a ridge of some height was thus formed and was traceable for a mile [1.6 km] along the river flat. Before reaching the hut most of the signs of earthquake action had died away…and we were now certainly beyond (to the north of) the line and belt of country most violently affected by the earthquakes…passing thus beyond the region visibly bearing traces of earthquake-action, we did not deem it necessary to proceed further in the direction of the Hope Saddle, and from the hut we returned to the junction of the Kiwi Creek with the Hope. We might have followed the earth-fractures, old and new, about a mile [~1.6 km] farther, to the edge of the bush on the east side of the low saddle already mentioned, but the day was passing and it was necessary to return to Glenwye (Glynn Wye) before dark…" (McKay, 1890, p. 12)

(14) "The mountain range lying between the low saddle mentioned and the source of the Hope River and Hope Saddle had on eastern spur one notably large slip and some of lesser size. The large slip looked to me as though it had been there before the earthquakes; but Mr. Rutherford, not having noted it previously, was of the opinion that it not only was caused by the earthquakes, but also that is happened right in the line of greater dislocation which we had followed more or less closely from Glenwye (Glynn Wye). In the Hope Valley…the mountains on both sides are marked by a great number of landslips that have taken place recently, and these were not observed previous to the beginning of September 1st…" (McKay, 1890, p. 11, 13)

(15) "The facts that I noted, in my opinion, tend to show that the great shock of the morning of the 1st September commenced at some point to the west of Glenwye (Glynn Wye), perhaps further west than the junction of the Kiwi with the Hope, and that it traveled east-ward with increasing force to Glenwye (Glynn Wye) and Hopefield (Glenhope), beyond which places, by what appears at the surface, its destructive character began to be less; and, although as far as the eastern end of the Hanmer Plain its violence was great, if rents and fissures are to be taken as a measure of its force, it was here mild and tame compared with what it was at the Hopefield (Glenhope) and Glenwye (Glynn Wye)…and though a number of small rents were formed along the bed of Percival River, clearly in this direction the power of the movement and force of its shock was being rapidly lessened, and not more than 10 miles [16 km] further to the east, between the Hanmer River and Lottery Creek, there is not the least indication of fresh disturbance along the old line of earthquake-rent." (McKay, 1890, p. 13)

(16) "After the earthquake we all learned that the earth fissure which commences at the Hanmer Plains, runs through my old place, and several miles of Glynn Wye, was an old earthquake crack. One side of this crack seemed to remain firm, while the other side shifted about five feet (1.5 m) further north. I knew this because I had a wire fence running from the hills in a straight line to the River Waiau" (Jones, 1933, p. 123) and, "At Jones's station, the old earthquake-rent passed on to a terrace of lower level, and we had less opportunity for observing it closely…" (McKay, 1890, p. 6)

(17) "…Mr. Thompson, of Glenwye, informed me that…though he cannot say that the great shock came from the west of Glenwye, it certainly passed down the valley eastward from that place at a measurable rate, and was accompanied by a terrific roaring noise, which died away in the distance, while things were momentarily quiet at the place where he stood" (McKay, 1890, p. 14)

APPENDIX 2. TRENCH UNIT DESCRIPTIONS

Trench unit descriptions for Hope Shelter trench 1 (February 2012), west wall, are given in Table A1. Trench unit descriptions for Hope Shelter trench 2 (February 2013), east wall, are given in Table A2.

APPENDIX 3. DETAILS OF OXCAL MODELING

Modeling Trench 1 Data

For modeling T-1, we used ages from samples HS1-25, HS1-3, HS1-22, HS1-4, HS1-7, HS1-11, HS1-13, and HS1-19 (Table 2). Nine samples were eliminated from the model because their ages were out of stratigraphic order, reversed, or considered to be modern or too young. Samples HS1-1, HS1-1/2, HS1-2, HS1-3, and HS1-23 are in a reverse order of age with respect to each other. Among these, we preferred to use sample HS1-3 because its age is concordant with the age of the upper peat (unit 10) in T-2. Samples HS1-20 and HS1-5 were considered to be out of stratigraphic order with the sequence in T-1, and on closer inspection, these samples were probably rooty materials. Sample HS1-16 included several different fragments indicating a younger age than sample HS1-13, which is in a higher stratigraphic position. Therefore, this sample was also not used.

Event horizons were identified between the dated samples based on our description in the section "Trench 1 Faulting." Because faulting of unit 2 was unclear, we constructed two models: (1) using six events (T-1 model 1) and (2) using five events (T-1 model 2). The command "Boundary" was applied to the top and bottom of the model, assuming that all events were equally likely to come anywhere within the sequence and to force OxCal to sample the sequence for the entire age range used within the sequence (Lienkaemper and Ramsey, 2009). The 1888 Amuri earthquake was placed in the OxCal model above E1 in T-1 model 1 in order to better constrain the timing of that event.

TABLE A1. TRENCH UNIT DESCRIPTIONS, HOPE SHELTER TRENCH 1 (FEBRUARY 2012), WEST WALL

Unit	Description	Interpretation
1	Top soil	Soil
1a	Light-brown nutty silt, abundant fine roots, massive	Light-gray-brown soil/subsoil
1p	Light-brown peaty silt, abundant fine roots and grass	Peaty soil
2	Medium-gray, moderately to poorly sorted, pebbly silty sand, max. clast size: 4 cm, moderately firm	Colluvial wedge
3	Dark-gray-brown, moderately to poorly sorted, sandy to pebbly peat, max. clast size: 1.5 cm, common plant fragments and stones	Stony peat/colluvium?
4	Dark-brown gritty peat, common root traces, max. clast size: 5 mm, moist, massive, spongy, silt texture peat	Peat
5	Dark-gray, moderately to poorly sorted, gravelly sandy silt, wet, max. clast size: 4 cm, average clast size: 1–2 cm, matrix: sandy silt	Alluvium/colluvium
6	Medium-gray gritty silty sand, max. clast size: 8 mm, include root fragments, soft, moist, sticky	Fine sand
6p	Light-gray-brown peat, abundant root fibers, soft, moist	Peat
7a	Medium-gray most silt, soft	Fine sandy silt
7p1 and 7p2	Thin rooty fibers	Thin peat stringers
7b	Reverse grading sequence of four subunits (b1: fine sandy silt, b2: medium to fine sand, b3: fine sand silt, b4: pebbly coarse sand [each layer is 2–3 cm thick])	Silty alluvium
8	Light reddish-gray silt with abundant peaty root fibers, moist soft and spongy, organic silt	Silt
8p	Red-brown fibrous peat	Peat
9	Reverse grading pair of subunits (9a: medium-brown gray organic silt [2 cm thick], moist, spongy; 9b: silty fine sand, light gray, well sorted [2 cm thick])	Alluvium
9p	Red fine fibrous peat	Peat
10	Medium-gray fine sandy silt, abundant peaty root traces, occasional plant fragments (leaf), moist	Silt
10p	Red-brown spongy fibrous peat	Peat
11	Normal grading sequence, package of light-gray stony silt at base (moderately sorted) to light-gray silt at top, top has some peaty root fibers (very well sorted), moist, soft	Silty alluvium
11p1 and 11p2	Light reddish-brown fine fibrous peat	Peat
12p	Thick red-brown peat	Peat
12a	Medium-gray coarse sand, max. clast size: 5 mm, well sorted, loose	Alluvial sand
13p	Red fine hairy peat	Peat
13	Light-gray clayey silt, moist	Silt
14	Light-gray clayey silt, moist	Silt
15	Medium-gray silty gravel, max. clast size: 15 cm, moderately to poorly sorted, average clast size: 2–3 cm, matrix: sandy silt	Alluvial gravel
18	Medium-gray stony fine sandy silt, max. clast size: 3 cm, average clast size: 1 cm, moist, slightly peaty with common peaty root fibrous	Sand, channel deposit
20	Light-brown-gray gravelly silt, max. clast size: 7 cm, average clast size: 2–3 cm, matrix: fine sandy silt with abundant fine roots, slight iron staining on clasts and roots	Colluvium
21	Medium-gray firm massive fine sandy silt, well sorted	Alluvial silt
22	Medium-brown gray clayey silt, massive, firm, clast orientation along a line	Alluvial silt
23	Light-brown-gray stony silt, max. clast size: 2 cm, moist, slightly firm, matrix: fine sandy silt	Faulted colluvium
25	Light-brown-gray sandy pebbly gravel, max. clast size: 10 cm, subangular, matrix: clayey silty sand, vertically oriented clasts	Faulted colluvium/shear zone
26	Light-gray silty gravel, wet, max. clast size: 12 cm, matrix: sandy silt	Shear zone
27	Light reddish-gray sandy gravel, max. clast size: 12 cm, oxidized graywacke clast, subangular to subrounded, matrix: medium to coarse sand	Faulted edge of fan deposits
28	Light reddish-gray pebbly silty sand, max. clast size: 7 cm, average clast size: 1 cm, moderately loose, matrix: loamy sand, some iron oxidation along root traces, gravelly loamy (clay, silt, sand) sand	Fan alluvium
28a	Gravelly silt, light-brown-gray, max. clast size: 11 cm, average clast size: 2–3 cm, matrix: fine sandy silt with abundant fine roots	Fan alluvium
29a	Light-olive-gray medium sand, well sorted, occasional pebbles up to 2 cm	Sand, channel deposit
29	Medium-olive-gray gravelly sand, max. clast size: 3 cm, average clast size: 8 mm, matrix: moderately loose	Sand, channel deposit
30a	Light-olive-gray sandy gravel, max. clast size: 18 cm, average clast size: 3 cm, matrix: medium-coarse sand, moderately loose, large clast iron stained	Fan alluvium
30b	Light reddish-gray gravelly sand, loose, moist, max. clast size: 15 cm, varies from poorly sorted to moderately sorted	Fan alluvium
30c	Dark-gray medium-coarse sand, very well sorted, moist	Fan alluvium

The command “Difference” was used to calculate the interevent intervals, and the command “RI” was used to calculate the distribution of the average recurrence between E1 and E6. The results are presented in Figures 12 and 13.

Modeling Trench 2 Data

For modeling T-2, we used ages from samples HS2-8, HS2-7, HS2-14, HS2-4, HS2-3, HS2-6, and HS2-1 (Table 2). Four samples were not used in the model. Sample HS2-11 has a modern age, and sample HS2-13 has an old age compared with other samples taken from below it. Sample HS2-9 comes from a very compact peat with no distinguishable organic macrofossils. This part of the stratigraphy at the northern end of T-2 appears to be interfingered and unconformable with the main sequence in the trench. Therefore, we suspect it is out of stratigraphic order and did not use it in the OxCal model. Samples HS2-1, HS2-2, and HS2-3 are at the bottom, middle, and top of unit 2, respectively. Sample HS2-2 is not in order with respect to the other two samples. Therefore, our preference is to use samples HS2-1 and HS2-3 because they come from stalky plant materials and seeds, which are more reliable, i.e., delicate, non-reworked fragments compared to other datable materials.

Event horizons were identified as specific stratigraphic levels between the dated samples based on our description in the section “Trench 2 Faulting.” As with the T-1 models, the commands “Boundary,” “Difference,” and “RI” were applied. The results are presented in Figure 14.

TABLE A2. TRENCH UNIT DESCRIPTIONS, HOPE SHELTER TRENCH 2 (FEBRUARY 2013), EAST WALL

Unit	Description	Interpretation
1	Light-gray clayey silt	Alluvial silt
2	Peat	Peat
2a	Peaty silt	Alluvial silt
3	Gritty fine sand	Alluvial sand
4	Peat	Peat
5	Moderately well-sorted, fine to medium sand with occasional root pieces, grading toward fault to fine muddy sand	Alluvial sand
6	Sandy pebble gravel, subangular to angular	Channel deposits
7	Medium-gray clayey fine sandy silt, common peaty roots	Alluvial silt
7pa	Peat	Peat
7pb	Peat stringer	Peat
8	Silty sandy pebble gravel, average clast size: 2 cm, max. clast size: 4 cm	Channel deposits
9	Medium-gray clayey silt, slightly gritty, abundant peaty roots	Alluvial silt
10	Light reddish-gray brown spongy silty peat, contains wood and plant fragments	Peat
11	Light-gray brown stony sandy silt, common fine roots	Stony swamp soil
12	Light-gray coarse sandy pebble gravel, firm, thins toward scarp	Channel gravel
13	Light-brown-gray organic silt, slightly stony, spongy, abundant fine roots	Peaty soil
20	Undifferentiated sandy gravel, average clast size: 5–7 cm, max. clast size: 20 cm, subangular to subrounded clasts, matrix: medium to coarse sand, matrix supported	Fan alluvium
21	Medium-gray silty clay	Faulted alluvium
21p	Peat stringer showing fault	Peat
22	Firm light-gray sandy silty clay with occasional pebbles	Marginal deposits/ faulted colluvium?
23	Medium-gray clayey silt	Faulted alluvium
24	Zone of medium-gray gritty silty clay with vertical fabric	Shear zone

ACKNOWLEDGMENTS

We wish to thank New Zealand Natural Hazards Research Platform for funding the light detection and ranging (LiDAR) project. We thank the Department of Geological Sciences, University of Canterbury, GHZ Paleoseismicity (GNS Science), and the New Zealand Earthquake Commission (EQC) for funding this research. We thank the Department of Conservation and the owner of Poplar Station, Kevin Henderson, for site access. We acknowledge Stefan Winkler for providing a Schmidt hammer and related academic discussions. We thank Sam McColl for reviewing this work and giving constructive comments. We acknowledge the reviewers and editors for their constructive comments to improve the manuscript. We also thank David Norton and Jarg Pettinga for their advice on dendrochronology and fault behavior.

REFERENCES CITED

Barka, A., 1996, Slip distribution along the North Anatolian fault associated with the large earthquakes of the period 1939 to 1967: Bulletin of the Seismological Society of America, v. 86, no. 5, p. 1238–1254.

Barka, A.A., and Kadinsky-Cade, K., 1988, Strike-slip fault geometry in Turkey and its influence on earthquake activity: Tectonics, v. 7, no. 3, p. 663–684, doi:10.1029/TC007i003p00663.

Barka, A., Akyüz, H.S., Altunel, E., Sunal, G., Çakir, Z., Dikbas, A., Yerli, B., Armijo, R., Meyer, B., De Chabalier, J.B., Rockwell, T., Dolan, J.R., Hartleb, R., Dawson, T., Christofferson, S., Tucker, A., Fumal, T., Langridge, R., Stenner, H., Lettis, W., Bachhuber, J., Page, W., 2002, The surface rupture and slip distribution of the 17 August 1999 İzmit earthquake (M 7.4), North Anatolian fault: Bulletin of the Seismological Society of America, v. 92, p. 43–60.

Barrell, D.J.A., and Townsend, D.B., 2012, General Distribution and Characteristics of Active Faults and Folds in the Hurunui District: North Canterbury GNS Science Consultancy Report 2012/113, 45 p.

Beauprêtre, S., Garambois, S., Manighetti, I., Malavieille, J., Sénéchal, G., Chatton, M., Davies, T., Larroque, C., Rousset, D., Cotte, N., and Romano, C., 2012, Finding the buried record of past earthquakes with GPR-based palaeoseismology: A case study on the Hope fault, New Zealand: Geophysical Journal International, v. 189, no. 1, p. 73–100, doi:10.1111/j.1365-246X.2012.05366.x.

Beavan, J., Tregoning, P., Bevis, M., Kato, T., and Meertens, C., 2002, Motion and rigidity of the Pacific plate and implications for plate boundary deformation: Journal of Geophysical Research, v. 107, no. B10, p. ETG19-1–ETG19-15, doi:10.1029/2001JB000282.

Ben-Zion, Y., and Rice, J.R., 1995, Slip patterns and earthquake populations along different classes of faults in elastic solids: Journal of Geophysical Research–Solid Earth, v. 100, no. B7, p. 12,959–12,983, doi:10.1029/94JB03037.

Berryman, K.R., 1984, Late Quaternary tectonics of New Zealand, *in* Walcott, R.W., compiler, An Introduction to the Recent Crustal Movements of New Zealand: The Royal Society of New Zealand Miscellaneous Series 7, p. 91–107.

Berryman, K.R., and Beanland, S., 1991, Variation in fault behaviour in different tectonic provinces of New Zealand: Journal of Structural Geology, v. 13, no. 2, p. 177–189, doi:10.1016/0191-8141(91)90065-Q.

Berryman, K.R., Rattenbury, M., Isaac, M., Villamor, P., and Van Dissen, R., 2003, Active faulting and strain at the junction of the Alpine and Hope faults, *in* Mortimer, N., and Lee, D., eds., GSNZ Inc 2003 Annual Conference, 1–4 December, University of Otago, Dunedin: Programme & Abstracts: Geological Society of New Zealand Miscellaneous Publication 116A, p. 18.

Berryman, K.R., Cochran, U.A., Clark, K.J., Biasi, G.P., Langridge, R.M., and Villamor, P., 2012, Major earthquakes occur regularly on an isolated plate boundary fault: Science, v. 336, no. 6089, p. 1690–1693, doi:10.1126/science.1218959.

Biasi, G.P., and Weldon, R., 1994, Quantitative refinement of calibrated ^{14}C distributions: Quaternary Research, v. 41, no. 1, p. 1–18, doi:10.1006/qres.1994.1001.

Biasi, G.P., and Weldon, R.J., 2009, San Andreas fault rupture scenarios from multiple paleoseismic records: Stringing pearls: Bulletin of the Seismological Society of America, v. 99, no. 2A, p. 471–498, doi:10.1785/0120080287.

Biasi, G.P., Weldon, R.J., Fumal, T.E., and Seitz, G.G., 2002, Paleoseismic event dating and the conditional probability of large earthquakes on the southern San Andreas fault, California: Bulletin of the Seismological Society of America, v. 92, no. 7, p. 2761–2781, doi:10.1785/0120000605.

Bowen, F.E., 1964, Sheet 15—Buller: Geological Map of New Zealand: Wellington, New Zealand, Department of Scientific and Industrial Research, scale 1:250,000.

Bronk Ramsey, C., 2013, OxCal Program, v. 4. 1. 7: Oxford, UK, Radiocarbon Accelerator Unit, University of Oxford, https://c14.arch.ox.ac.uk/oxcal.html (last accessed on 30 July 2012).

Clark, K.J., Cochran, U.A., Berryman, K.R., Biasi, G., Langridge, R., Villamor, P., Bartholomew, T., Litchfield, N., Pantosti, D., Marco, S., Van Dissen, R., Turner, G., and Hemphill-Haley, M., 2013, Deriving a long paleoseismic record from a shallow-water Holocene basin next to the Alpine fault, New Zealand: Geological Society of America Bulletin, v. 125, no. 5–6, p. 811–832, doi:10.1130/B30693.1.

Clayton, L., 1966, Tectonic depressions along the Hope fault, a transcurrent fault in North Canterbury, New Zealand: New Zealand Journal of Geology and Geophysics, v. 9, no. 1–2, p. 95–104, doi:10.1080/00288306.1966.10420198.

Cowan, H.A., 1989, An Evaluation of the Late Quaternary Displacements and Seismic Hazard Associated with the Hope and Kakapou Faults, Amuri District, North Canterbury [M.S. thesis]: Christchurch, University of Canterbury, 239 p.

Cowan, H.A., 1990, Late Quaternary displacements on the Hope fault at Glynn Wye, North Canterbury: New Zealand Journal of Geology and Geophysics, v. 33, no. 2, p. 285–293.

Cowan, H.A., 1991, The North Canterbury earthquake of September 1, 1888: Journal of the Royal Society of New Zealand, v. 21, p. 1–12, doi:10.1080/03036758.1991.10416105.

Cowan, H.A., and McGlone, M.S., 1991, Late Holocene displacements and characteristic earthquakes on the Hope River segment of the Hope fault, New Zealand: Journal of the Royal Society of New Zealand, v. 21, no. 4, p. 373–384, doi:10.1080/03036758.1991.10420834.

DeMets, C., Gordon, R.G., Argus, D.F., and Stein, S., 1994, Effect of recent revisions to the geomagnetic reversal time scale on estimates of current plate motions: Geophysical Research Letters, v. 21, no. 20, p. 2191–2194, doi:10.1029/94GL02118.

DeMets, C., Gordon, R.G., and Argus, D.F., 2010, Geologically current plate motions: Geophysical Journal International, v. 181, no. 1, p. 1–80, doi:10.1111/j.1365-246X.2009.04491.x.

Elliott, A.J., Dolan, J.F., and Oglesby, D.D., 2009, Evidence from coseismic slip gradients for dynamic control on rupture propagation and arrest through stepovers: Journal of Geophysical Research–Solid Earth, v. 114, no. B2, p. B02313, doi:10.1029/2008JB005969.

Eusden, J.D., Pettinga, J.R., and Campbell, J.K., 2000, Structural evolution and landscape development of a collapsed transpressive duplex on the Hope fault, North Canterbury, New Zealand: New Zealand Journal of Geology and Geophysics, v. 43, no. 3, p. 391–404, doi:10.1080/00288306.2000.9514896.

Eusden, J.D., Pettinga, J.R., and Campbell, J.K., 2005, Structural collapse of a transpressive hanging-wall fault wedge, Charwell region of the Hope fault, South Island, New Zealand: New Zealand Journal of Geology and Geophysics, v. 48, no. 2, p. 295–309, doi:10.1080/00288306.2005.9515116.

Freund, R., 1971, The Hope Fault: A Strike-Slip Fault in New Zealand: New Zealand Geological Survey Bulletin 86, 49 p.

Fumal, T.E., Weldon, R.J., Biasi, G.P., Dawson, T.E., Seitz, G.G., Frost, W.T., and Schwartz, D.P., 2002, Evidence for large earthquakes on the San Andreas fault at the Wrightwood, California, paleoseismic site: A.D. 500 to present: Bulletin of the Seismological Society of America, v. 92, no. 7, p. 2726–2760, doi:10.1785/0120000608.

Grant, L.B., and Sieh, K., 1994, Paleoseismic evidence of clustered earthquakes on the San Andreas fault in the Carrizo Plain, California: Journal of Geophysical Research–Solid Earth, v. 99, no. B4, p. 6819–6841, doi:10.1029/94JB00125.

Gregg, D.R., 1964, Sheet 18—Hurunui: Geological Map of New Zealand: Wellington, New Zealand, Department of Scientific and Industrial Research, scale 1:250,000.

Hartleb, R.D., Dolan, J.F., Akyüz, H.S., Dawson, T.E., Tucker, A.Z., Yerli, B., Rockwell, T.K., Toraman, E., Çakir, Z., Dikbaş, A., and Altunel, E., 2002, Surface rupture and slip distribution along the Karadere segment of the 17 August 1999 İzmit and the western section of the 12 November 1999 Düzce, Turkey, earthquakes: Bulletin of the Seismological Society of America, v. 92, no. 1, p. 67–78, doi:10.1785/0120000829.

Hartleb, R.D., Dolan, J.F., Akyüz, H.S., and Yerli, B., 2003, A 2000-year-long paleoseismologic record of earthquakes along the central North Anatolian fault, from trenches at Alayurt, Turkey: Bulletin of the Seismological Society of America, v. 93, no. 5, p. 1935–1954, doi:10.1785/0120010271.

Hartleb, R.D., Dolan, J.F., Kozaci, Ö., Akyüz, H.S., and Seitz, G.G., 2006, A 2500-yr-long paleoseismologic record of large, infrequent earthquakes on the North Anatolian fault at Çukurçimen, Turkey: Geological Society of America Bulletin, v. 118, no. 7–8, p. 823–840, doi:10.1130/B25838.1.

Hogg, A., Hua, Q., Blackwell, P, Niu, M., Buck, C., Guilderson, T., Heaton, T., Palmer, J., Reimer, P., Reimer, R., Turney, C.., Zimmerman, S., 2013, SHCal13 Southern Hemisphere Calibration, 0-50,000 years cal B.P. Radiocarbon, v. 55(4), p. 1889–1903.

Howarth, J.D., Fitzsimons, S.J., Norris, R.J., and Jacobsen, G.E., 2014, Lake sediments record high intensity shaking that provides insight into the location and rupture length of large earthquakes on the Alpine fault, New Zealand: Earth and Planetary Science Letters, v. 403, p. 340–351, doi:10.1016/j.epsl.2014.07.008.

Jones, E., 1933, Autobiography of an Early Settler in New Zealand: Wellington, New Zealand, Coulls Somerville Wilkie Ltd, 179 p.

Kanamori, H., 1977, The energy release in great earthquakes: Journal of Geophysical Research, v. 82, p. 2981–2987, doi:10.1029/JB082i020p02981.

Khajavi, N., 2015, Surface Rupture Morphology and Paleoseismology of the Western Hope Fault and Characteristics of Seismically-Displaced Boulders in the Port Hills, South Island, New Zealand [Ph.D. thesis]: Christchurch, University of Canterbury.

Khajavi, N., Langridge, R., and Quigley, M., 2012, New insights into the rupture history of the Hope fault, New Zealand: San Francisco, California, American Geophysical Union, Fall Meeting supplement, abstract T21H-03.

Khajavi, N., Quigley, M., and Langridge, R.M., 2014, Influence of topography and basement depth on surface rupture morphology revealed from LiDAR and field mapping, Hope fault, New Zealand: Tectonophysics, v. 630, p. 265–284.

Knuepfer, P.L.K., 1984, Tectonic Geomorphology and Present-Day Tectonics of the Alpine Shear System, South Island, New Zealand (Neotectonics, Faults) [Ph.D thesis]: Tucson, Arizona, University of Arizona, 489 p.

Knuepfer, P.L.K., 1992, Temporal variations in latest Quaternary slip across the Australian- Pacific plate boundary, northeastern South Island, New Zealand: Tectonics, v. 11, no. 3, p. 449–464, doi:10.1029/91TC02890.

Langridge, R.M., and Berryman, K.R., 2005, Morphology and slip rate of the Hurunui section of the Hope fault, South Island, New Zealand: New Zealand Journal of Geology and Geophysics, v. 48, no. 1, p. 43–57, doi:10.1080/00288306.2005.9515097.

Langridge, R.M., Stenner, H.D., Fumal, T.E., Christofferson, S.A., Rockwell, T.K., Hartleb, R.D., Bachhuber, J., and Barka, A.A., 2002, Geometry, slip distribution, and kinematics of surface rupture on the Sakarya fault segment during the 17 August 1999 İzmit, Turkey, earthquake: Bulletin of the Seismological Society of America, v. 92, no. 1, p. 107–125, doi:10.1785/0120000804.

Langridge, R.M., Campbell, J., Hill, N., Pere, V., Pope, J., Pettinga, J., Estrada, B., and Berryman, K., 2003, Paleoseismology and slip rate of the Conway segment of the Hope fault at Greenburn Stream, South Island, New Zealand: Annals of Geophysics, v. 46, no. 5, p. 1119–1140.

Langridge, R.M., Duncan, R., and Almond, P., 2007, Indicators of Recent Paleoseismic Activity along the Western Hope Fault: GNS Science Consultancy Report 2006/151, 99 p. + appendices.

Langridge, R.M., Almond, P.C., and Duncan, R.P., 2013, Timing of late Holocene paleoearthquakes on the Hurunui segment of the Hope fault: Implications for plate boundary strain release through South Island, New Zealand: Geological Society of America Bulletin, v. 125, no. 5–6, p. 756–775, doi:10.1130/B30674.1.

Langridge, R.M., Ries, W.F., Farrier, T., Barth, N.C., Khajavi, N., and De Pascale, G.P., 2014, Developing sub 5-m LiDAR DEMs for forested sections of the Alpine and Hope faults, South Island, New Zealand: Implications for structural interpretations: Journal of Structural Geology, v. 64, p. 53–66.

Lensen, G.J., 1962, Sheet 16—Kaikoura: Geological Map of New Zealand: Wellington, New Zealand, Department of Scientific and Industrial Research, scale 1:250,000.

Leonard, M., 2010, Earthquake fault scaling: Self-consistent relating of rupture length, width, average displacement, and moment release: Bulletin of the Seismological Society of America, v. 100, no. 5A, p. 1971–1988, doi:10.1785/0120090189.

Lienkaemper, J.J., and Ramsey, C.B., 2009, OxCal: Versatile tool for developing paleoearthquake chronologies—A primer: Seismological Research Letters, v. 80, no. 3, p. 431–434, doi:10.1785/gssrl.80.3.431.

Lin, A., Rao, G., and Yan, B., 2012, Field evidence of rupture of the Qingchuan fault during the 2008 Mw7.9 Wenchuan earthquake, northeastern segment of the Longmen Shan thrust belt, China: Tectonophysics, v. 522–523, p. 243–252, doi:10.1016/j.tecto.2011.12.012.

McCalpin, J.P., 2009, Paleoseismology (2nd ed.): Burlington, Massachusetts, Elsevier Science, 848 p.

McKay, A., 1890, On the Earthquakes of September 1888 in the Amuri and Marlborough Districts of the South Island: New Zealand Geological Survey Report of Geological Explorations 20, p. 1–16.

McKay, A., 1902, Report on the Recent Seismic Disturbances within Cheviot County in Northern Canterbury and the Amuri District of Nelson, New Zealand (November and December, 1901): Wellington, New Zealand, Government Printer, 80 p.

Nathan, S., Rattenbury, M.R., and Suggate, R.P., 2002, Geology of the Greymouth Area: Lower Hutt, New Zealand, Institute of Geological and Nuclear Sciences Geological Map 12, scale 1:250,000, 58 p. + 1 folded map.

Oglesby, D.D., 2005, The dynamics of strike-slip step-overs with linking dip-slip faults: Bulletin of the Seismological Society of America, v. 95, no. 5, p. 1604–1622, doi:10.1785/0120050058.

Pettinga, J.R., Yetton, M.D., Van Dissen, R.J., and Downes, G., 2001, Earthquake source identification and characterisation for the Canterbury region, South Island, New Zealand: Bulletin of the New Zealand Society for Earthquake Engineering, v. 34, no. 4, p. 282–317.

Quigley, M., Van Dissen, R., Litchfield, N., Villamor, P., Duffy, B., Barrell, D., Furlong, K., Stahl, T., Bilderback, E., and Noble, D., 2012, Surface rupture during the 2010 Mw 7.1 Darfield (Canterbury) earthquake: Implications for fault rupture dynamics and seismic-hazard analysis: Geology, v. 40, no. 1, p. 55–58, doi:10.1130/G32528.1.

Rattenbury, M.S., Townsend, D., and Johnston, M.R., 2006, Geology of the Kaikoura Area: Lower Hutt, New Zealand, GNS Science/Institute of Geological and Nuclear Sciences Geological Map 13, scale 1:250,000, 70 p. + 1 folded map.

Rockwell, T.K., Lindvall, S., Herzberg, M., Murbach, D., Dawson, T., and Berger, G., 2000, Paleoseismology of the Johnson Valley, Kickapoo, and Homestead Valley faults: Clustering of earthquakes in the Eastern California shear zone: Bulletin of the Seismological Society of America, v. 90, no. 5, p. 1200–1236, doi:10.1785/0119990023.

Scharer, K.M., Weldon Ii, R.J., Fumal, T.E., and Biasi, G.P., 2007, Paleoearthquakes on the southern San Andreas fault, Wrightwood, California, 3000 to 1500 B.C.: A new method for evaluating paleoseismic evidence and earthquake horizons: Bulletin of the Seismological Society of America, v. 97, no. 4, p. 1054–1093, doi:10.1785/0120060137.

Seitz, G., Weldon, I.I.R., and Biasi, G.P., 1997, The Pitman Canyon paleoseismic record: A re-evaluation of southern San Andreas fault segmentation: Journal of Geodynamics, v. 24, no. 1–4, p. 129–138, doi:10.1016/S0264-3707(96)00042-7.

Seitz, G.G., Biasi, G.P., and Weldon, R.J., 2013, An improved paleoseismic record of the San Andreas fault at Pitman Canyon, *in* Noller, J.S., Sowers, J.M., and Lettis, W.R., eds., Quaternary Geochronology: Methods and Applications: American Geophysical Union Reference Shelf 4, p. 563–566.

Stahl, T., Winkler, S., Quigley, M., Bebbington, M., Duffy, B., and Duke, D., 2013, Schmidt hammer exposure-age dating (SHD) of late Quaternary fluvial terraces in New Zealand: Earth Surface Processes and Landforms, v. 38, no. 15, p. 1838–1850, doi:10.1002/esp.3427.

Stirling, M., McVerry, G., Gerstenberger, M., Litchfield, N., Van Dissen, R., Berryman, K., Barnes, P., Wallace, L., Villamor, P., Langridge, R., Lamarche, G., Nodder, S., Reyners, M., Bradley, B., Rhoades, D., Smith, W., Nicol, A., Pettinga, J., Clark, K., and Jacobs, K., 2012, National seismic hazard model for New Zealand: 2010 update: Bulletin of the Seismological Society of America, v. 102, no. 4, p. 1514–1542, doi:10.1785/0120110170.

Vallée, M., and Satriano, C., 2014, Ten year recurrence time between two major earthquakes affecting the same fault segment: Geophysical Research Letters, v. 41, no. 7, p. 2312–2318, doi:10.1002/2014GL059465.

Van Dissen, R., 1989, Late Quaternary Faulting in the Kaikoura Region, Southeastern Marlborough, New Zealand [M.S. thesis]: Corvallis, Oregon State University, 72 p.

Van Dissen, R., and Yeats, R.S., 1991, Hope fault, Jordan thrust, and uplift of the Seaward Kaikoura Range, New Zealand: Geology, v. 19, no. 4, p. 393–396, doi:10.1130/0091-7613(1991)019<0393:HFJTAU>2.3.CO;2.

Wallace, L.M., Beavan, J., McCaffrey, R., Berryman, K., and Denys, P., 2007, Balancing the plate motion budget in the South Island, New Zealand, using GPS, geological and seismological datas: Geophysical Journal International, v. 168, no. 1, p. 332–352, doi:10.1111/j.1365-246X.2006.03183.x.

Wallace, L.M., Barnes, P., Beavan, J., Van Dissen, R., Litchfield, N., Mountjoy, J., Langridge, R., Lamarche, G., and Pondard, N., 2012, The kinematics of a transition from subduction to strike-slip: An example from the central New Zealand plate boundary: Journal of Geophysical Research–Solid Earth, v. 117, no. B2, 24 p.

Warren, G., 1967, Sheet 17—Hokitika: Geological Map of New Zealand: Wellington, New Zealand, Department of Scientific and Industrial Research, scale 1:250,000.

Weldon, R.J., Fumal, T.E., Biasi, G.P., and Scharer, K.M., 2005, Past and future earthquakes on the San Andreas fault: Science, v. 308, no. 5724, p. 966–967, doi:10.1126/science.1111707.

Wells, D.L., and Coppersmith, K.J., 1994, New empirical relationships among magnitude, rupture length, rupture width, rupture area, and surface displacement: Bulletin of the Seismological Society of America, v. 84, no. 4, p. 974–1002.

Wesnousky, S.G., 1988, Seismological and structural evolution of strike-slip faults: Nature, v. 335, no. 6188, p. 340–343, doi:10.1038/335340a0.

Wesnousky, S.G., 2006, Predicting the endpoints of earthquake ruptures: Nature, v. 444, no. 7117, p. 358–360, doi:10.1038/nature05275.

Wesnousky, S.G., 2008, Displacement and geometrical characteristics of earthquake surface ruptures: Issues and implications for seismic-hazard analysis and the process of earthquake rupture: Bulletin of the Seismological Society of America, v. 98, no. 4, p. 1609–1632, doi:10.1785/0120070111.

Wesnousky, S.G., and Biasi, G.P., 2011, The length to which an earthquake will go to rupture: Bulletin of the Seismological Society of America, v. 101, p. 1948–1950, doi:10.1785/0120110013.

Wood, R.A., Pettinga, J.R., Bannister, S., Lamarche, G., and McMorran, T.J., 1994, Structure of the Hanmer strike-slip basin, Hope fault, New Zealand: Geological Society of America Bulletin, v. 106, no. 11, p. 1459–1473, doi:10.1130/0016-7606(1994)106<1459:SOTHSS>2.3.CO;2.

Yang, J.S., 1991, The Kakapo fault—A major active dextral fault in the central North Canterbury–Buller regions of New Zealand: New Zealand Journal of Geology and Geophysics, v. 34, no. 2, p. 137–143, doi:10.1080/00288306.1991.9514451.

Yeats, R.S., and Berryman, K.R., 1987, South Island, New Zealand, and Transverse Ranges, California: A seismotectonic comparison (USA): Tectonics, v. 6, no. 3, p. 363–376, doi:10.1029/TC006i003p00363.

Science Editor: David I. Schofield
Associate Editor: Erin K. Beutel

Manuscript Received 3 September 2014
Revised Manuscript Received 12 April 2016
Manuscript Accepted 9 June 2016

Printed in the USA